

EXPLORING CORROSION INHIBITION PROPERTIES OF  
THIADIAZOL COMPOUND FOR THE PROTECTION OF CARBON  
STEEL

by

Sabiha Sharmin

MASTER OF SCIENCE IN CHEMISTRY



DEPARTMENT OF CHEMISTRY

BANGLADESH UNIVERSITY OF ENGINEERING AND TECHNOLOGY

DHAKA, BANGLADESH

APRIL, 2023

Exploring Corrosion Inhibition Properties of Thiadiazol Compound for  
the Protection of Carbon Steel

by

Sabiha Sharmin

A thesis submitted to the

Department of Chemistry

in partial fulfillment for the degree of

MASTER OF SCIENCE IN CHEMISTRY



Department of Chemistry

Bangladesh University of Engineering and Technology

Dhaka, Bangladesh

April 2023



**Department of Chemistry**  
**Bangladesh University of Engineering and Technology (BUET)**

The thesis titled “EXPLORING CORROSION INHIBITION PROPERTIES OF THIADIAZOL COMPOUND FOR THE PROTECTION OF CARBON STEEL” submitted by **Sabiha Sharmin**, Student ID- **0419032701**, has been accepted *Satisfactory* in partial fulfillment of the requirement for the degree of **Master of Science in Chemistry** on **10<sup>th</sup> April 2023**.

**Board of Examiners**

1. Dr. Chanchal Kumar Roy  
Assistant Professor  
Department of Chemistry  
BUET, Dhaka

Chairman  
(Supervisor)

2. Dr. Al-Nakib Chowdhury  
Professor and Head  
Department of Chemistry  
BUET, Dhaka

Member  
(Ex-Officio)

3. Dr. Md. Nazrul Islam  
Professor  
Department of Chemistry  
BUET, Dhaka

Member

4. Dr. Shimul Saha  
Assistant Professor  
Department of Chemistry  
BUET, Dhaka

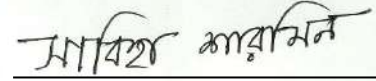
Member

5. Dr. Hossain Mohammad Mamun Al Rashed  
Associate Professor  
Department of Materials and Metallurgical Engineering  
BUET, Dhaka

Member  
(External)

## DECLARATION

I hereby declare that this thesis is my own work and to the best of my knowledge it contains no materials previously published or written by another person, or have been accepted for the award of any other degree or diploma at Bangladesh University of Engineering and Technology (BUET) or any other educational institution, except where due acknowledgment is made. I also declare that the intellectual content of this thesis is the product of my own work and any contribution made to the research by others, with whom I have worked at BUET or elsewhere, is explicitly acknowledged.



Sabiha Sharmin

Dedicated to.....

---

*My Beloved Family*

*&*

*Advanced Research Laboratory*

---

## TABLE OF CONTENTS

Table of content.....	v
List of figures and Tables.....	viii
List of Abbreviations of Technical Symbols and Terms.....	xi
Acknowledgment.....	xii
Abstract.....	xiv

### 1. Chapter

1.1 General Introduction .....	2
1.2 The objective of this work .....	3
1.3 Carbon Steel.....	3
1.4 Corrosion.....	4
1.5 Economic Aspects of Corrosion .....	4
1.6 Types of Corrosion .....	5
1.6.1 General Corrosion.....	5
1.6.2 Pitting Corrosion.....	5
1.6.3 Dealloying, Dezincification and Parting.....	6
1.6.4 Intergranular Corrosion.....	6
1.6.5 Stress-Corrosion Cracking .....	6
1.6.6 Galvanic Corrosion .....	6
1.6.7 Crevice Corrosion .....	6
1.6.8 Corrosion Fatigue.....	7
1.6.9 Fretting Corrosion.....	7
1.7 Electrochemical Principals of Corrosion .....	7
1.8 Corrosion Inhibitors .....	9
1.9 Thiadiazole Derivatives .....	10
1.10 Synergistic Effect on Organic Corrosion Inhibitors .....	12
1.11 Adsorption Phenomenon of CI on Metal Surface.....	13
1.12 Theories of Experimental Techniques .....	13
1.13 Weight-loss Measurement .....	13

1.14 Scanning Electron Microscopy (SEM) .....	14
1.15 Adsorption Isotherm and Thermodynamic Characterization.....	14
1.16 Thermodynamic Parameters .....	15
1.16 Electrochemical Techniques .....	16
1.16.1 Open Circuit Potential.....	16
1.16.2 Potentiodynamic Polarization .....	18
1.16.3 Electrochemical Impedance Spectroscopy .....	19
References.....	21

## 2. Chapter

2.1 Chemicals & Reagents.....	27
2.2 Synthesis of 2-amino-5-(4-nitrophenyl)-1,3,4-thiadiazole (ANPT) .....	27
2.3 Method of Solution Preparation.....	27
2.3.1 Preparation of Stock Solution of HCl .....	28
2.3.2 Preparation of CTAB solution .....	28
2.3.3 Preparation of ANPT solution .....	28
2.4 Instruments.....	28
2.5 Cells and Electrodes.....	28
2.6 Preparation of Working Electrode .....	29
2.7 Test Method .....	30
2.7.1 WL Measurement.....	30
2.7.2 Surface Analysis .....	30
2.7.3 Electrochemical Analysis.....	30
2.7.3.1 OCP.....	30
2.7.3.2 PDP .....	30
2.7.3.3 EIS Measurement.....	31
Reference .....	32

## 3. Chapter

3.1 Synthesis of 2-amino-5-(4-nitrophenyl)-1,3,4-thiadiazole (ANPT) .....	34
3.2 Weight-Loss Test.....	37
3.3 FE-SEM Analysis of CS Surfaces: .....	37
3.4 Adsorption Isotherm .....	39
3.5 Thermodynamic Characterization.....	45
3.6 Electrochemical Studies.....	49
3.7 OCP Analysis.....	49
3.8 PDP Analysis .....	51
3.9 EIS Analysis.....	52

3.10 Synergistic Effect in Presence of Surfactant.....	55
3.10.1 OCP Analysis.....	55
3.10.2 PDP Analysis .....	56
3.10.3 FE-SEM Analysis of CS Surfaces .....	58
3.11 Proposed Corrosion Inhibition Mechanism .....	59
References.....	62
<b>4. Chapter</b>	
4.1 Conclusion: .....	68



## List of Figures and Tables

### Figures

<b>Figure 1. 1</b>	The chemical structure of 2-amino-1,3,4-thiadiazole.....	3
<b>Figure 1. 2</b>	Pitting corrosion on CS.....	5
<b>Figure 1. 3</b>	Rust formation on CS in the presence of water and air .....	9
<b>Figure 1. 4</b>	Structures of surfactants, (a) CTAB and (b) SDS. ....	12
<b>Figure 1. 5</b>	EDL .....	17
<b>Figure 1. 6</b>	Schematic diagram of OCP plot .....	17
<b>Figure 1. 7</b>	Schematic diagram of Tafel plot .....	18
<b>Figure 1. 8</b>	Schematic diagram of Nyquist plot and Bode plot.....	20
<b>Figure 2. 1</b>	Synthesis route of 2-amino-5-(4-nitrophenyl)-1,3,4-thiadiazole (ANPT)27	
<b>Figure 2. 2</b>	Three-electrode system.....	29
<b>Figure 2. 3</b>	Working electrode (CS).....	29
<b>Figure 3. 1</b>	Synthesis route of 2-amino-5-(4-nitrophenyl)-1,3,4-thiadiazole (ANPT)34	
<b>Figure 3. 2</b>	FT- IR spectrum of ANPT.....	35
<b>Figure 3. 3</b>	NMR Spectra of ANPT (a) NMR spectra (b) expanded NMR spectra ....	36
<b>Figure 3. 4</b>	SEM images of CS surface (a) before immersion (b) corroded surface after immersion 0.5 M HCl solution (c) in presence of 200 ppm ANPT .....	38
<b>Figure 3. 5</b>	Langmuir adsorption model of various concentrations of ANPT on the surface of CS in 0.5 M HCl at different temperatures .....	40
<b>Figure 3. 6</b>	Temkin isotherm adsorption model of various concentrations of ANPT on the surface of CS in 0.5 M HCl at different temperatures .....	42
<b>Figure 3. 7</b>	Freundlich isotherm adsorption model of various concentrations of ANPT on the surface of CS in 0.5 M HCl at different temperatures .....	44
<b>Figure 3. 8</b>	Arrhenius Plot for CS in 0.5 M HCl solution without and with ANPT at different concentrations of ANPT.....	46
<b>Figure 3. 9</b>	Alternative Arrhenius Plot of $\ln(CR/T)$ vs. $1000/T$ for CS in 0.5 M HCl solution without and with different concentrations of ANPT.....	47
<b>Figure 3. 10</b>	Time variation of the OCP for CS in 0.5 M HCl solution with different concentrations of ANPT at room temperature .....	50
<b>Figure 3. 11</b>	PDP plots for CS in 0.5 M HCl solution with different concentrations of ANPT at room temperature.....	51
<b>Figure 3. 12</b>	Nyquist plots for CS in 0.5 M HCl with different concentrations of ANPT .....	53
<b>Figure 3. 13</b>	Bode plots for CS in 0.5 M HCl with different concentrations of ANPT .....	53
<b>Figure 3. 14</b>	Equivalent circuit.....	54

<b>Figure 3. 15</b> Time variation of the OCP for CS in 0.5 M HCl solution with different concentrations of ANPT in combination with 1 mM CTAB at room temperature .....	55
<b>Figure 3. 16</b> PDP plots for CS in 0.5 M HCl solution with different concentrations of ANPT in presence of 1 mM CTAB at room temperature .....	57
<b>Figure 3. 17</b> SEM of CS surface (a) before immersion (b) corroded surface after immersion 0.5 M HCl solution (c) in presence of 200 ppm ANPT (d) in presence of 200 ppm along with 1 mM CTAB .....	59
<b>Figure 3. 18</b> Inhibition mechanism of ANPT on the CS surface against HCl .....	61
<b>Figure 3. 19</b> Inhibition mechanism of ANPT on the CS surface in presence of CTAB against HCl.....	61

## Tables

<b>Table 1. 1</b> Structure of some developed thiadiazole derivatives as corrossions inhibitor .....	11
<b>Table 3. 1</b> Corrosion parameters for CS immersed in 0.5M HCl solution for 3h without/with different concentrations of ANPT at 298 K temperature obtained from WL measurements.....	37
<b>Table 3. 2</b> The values of $C_{inh}$ and $\theta$ at different temperatures .....	39
<b>Table 3. 3</b> Adsorption parameters of ANPT and CS surface in 0.5 M HCl by Langmuir adsorption isotherm at different temperatures (298 K, 303 K, 313 K, 323 K) .....	41
<b>Table 3. 4</b> The values of $C_{inh}$ , $\ln C_{inh}$ and $\theta$ at different temperatures .....	41
<b>Table 3. 5</b> Adsorption parameters of ANPT and CS surface in 0.5 M HCl by Temkin adsorption isotherm at different temperatures (298 K, 303 K, 313 K, 323 K) .....	42
<b>Table 3. 6</b> The values of $C_{inh}$ , $\ln C_{inh}$ and $\theta$ at different temperatures .....	43
<b>Table 3. 7</b> Adsorption parameters of ANPT and CS surface in 0.5M HCl by Freundlich adsorption isotherm at different temperatures (298K, 303K, 313K, 323K) .....	44
<b>Table 3. 8</b> Corrosion parameters for CS immersed in 0.5 M HCl solution for 3 hours without/with ANPT at 298 K, 303 K, 313 K & 323 K temperature obtained from WL measurements.....	45
<b>Table 3. 9</b> The activation energy of adsorption on the CS surface in the absence and presence of ANPT at different concentrations was calculated by Arrhenius Plot.....	46
<b>Table 3. 10</b> Some thermodynamic parameters for the adsorption of ANPT on the CS surface .....	48
<b>Table 3. 11</b> The PDP parameters for CS in 0.5 M HCl solution without/with different concentrations of ANPT at room temperature .....	52
<b>Table 3. 12</b> Electrochemical impedance parameters for CS in 0.5 M HCl solution with ANPT at different concentrations .....	54
<b>Table 3. 13</b> The PDP parameters for CS in 0.5M HCl solution with different concentrations of ANPT in presence of 1 mM CTAB at room temperature .....	57

## List of Abbreviation

1. CS: Carbon steel
2. CI: Corrosion inhibitor
3. CR: *CR*
4. ANPT: 2-amino-5-(4-nitrophenyl)-1,3,4-thiadiazole
5. OCP: Open circuit potential
6. PDP: Potentiodynamic polarization
7. EIS: Electrochemical impedance spectroscopy
8. WL: Weight-loss Test
9. SEM: Scanning electron microscopy
10. EDX: Energy dispersive X-ray
11. WE: Working electrode
12. CE: Counter electrode
13. RE: Reference electrode
14.  $i_{\text{corr}}$ : Corrosion current
15.  $E_{\text{corr}}$ : Corrosion potential
16.  $IE\%$ : *IE*
17.  $R_f$ : Solution resistance
18.  $R_t$ : Charge transfer resistance
19. EDL: Electrical Double Layer

## **Acknowledgement**

At the very beginning. I humbly acknowledge my deepest gratitude to the almighty, the most gracious, benevolent and merciful creator for his infinite mercy bestowed on me in carrying out the research work presented in the dissertation.

It is a great pleasure for me to acknowledge my deepest sense of gratitude, sincere appreciation, heartfelt indebtedness and solemn regards to my reverend teacher and supervisor, Assistant Professor, Department of Chemistry, Bangladesh University of Engineering and Technology (BUET), for his kind supervision, indispensable guidance, valuable and constructive suggestions, liberal help and continuous encouragement during the whole period. It is obvious that his attributive contribution and efforts have greatly shaped me into what I am today. In fact. I am quite fortunate to be a part of his ambitious research team.

It is my great honor to convey my sincere gratitude to my respected teacher Professor Dr. Al-Nakib Chowdhury, honorable Head of the Department of Chemistry, BUET for giving me his wonderful support to move through the academic processes during this M.Sc. program. I am thankful to all other respected teachers of the Department of Chemistry, BUET, for their time-to-time support. I would also like to thank all of the officers and staffs of the Department of Chemistry, BUET for their continuous help during my study period.

I am highly grateful to all members of the board of examiners for their valuable suggestions and resourceful comments.

I am thankful to my dear colleagues and all the members of Advance Research Laboratory for their friendly cooperation and lovely encouragement throughout my research period. Special thanks to Sharmin Sultana, Sabikun Nahar Munna, Md. Mahamudul Hasan Rumon & Anas Mahmud for their continuous help during the research. I am also thankful to other fellows of Chemistry Advance Research lab for

their cooperation during the research period. I am grateful to the authority of Bangladesh University of Engineering and Technology (BUET), Ministry of Science & Technology, Govt. of the People's Republic of Bangladesh for providing financial support for this research work.

Finally, I would like to express my heartfelt indebtedness and profound gratitude to my beloved father, mother and all of my family members for their continuous inspiration and immeasurable sacrifices throughout the period of my study. And heartiest thanks to my husband for his supports and encouragement.

10<sup>th</sup> April, 2023

Sabiha Sharmin

## ABSTRACT

Thiadiazole derivatives have gained much attention as non-volatile, non-flammable, and non-toxic corrosion inhibitors to build an eco-friendly world. However, these derivatives have found limited practical use for their low aqueous solubility and *IE*. Here, a water-soluble thiadiazole derivative 2-amino-5-(4-nitrophenyl)-1,3,4-thiadiazole (ANPT) has been synthesized, and its corrosion inhibition behavior has been investigated. A facile one-pot synthesis route has been followed for the synthesis. Fourier-transform infrared spectroscopy and nuclear magnetic resonance spectroscopy have been used to confirm the preparation of ANPT. The corrosion inhibition property of ANPT was investigated for carbon steel specimens in aqueous hydrochloric acid as corrosive media. Electrochemical techniques, open circuit potential measurement, potentiodynamic polarization and impedance spectroscopy were used to determine the corrosion *IE*. Weight-loss measurement was carried out to investigate the practical inhibition situation. Scanning electron microscopic images, before and after the corrosion, were analyzed to observe the changes in surface microstructure during corrosion. The experimental results of electrochemical tests showed that ANPT is a suitable corrosion inhibitor for carbon steel with 56 % corrosion *IE* against the highly corrosive 0.5 M HCl solution. The maximum *IE* has been observed at a concentration of 200 ppm. The ANPT protects carbon steel from corrosion by physical adsorption. The high *IE* was attributed to the blocking of active sites by the adsorption of inhibitor molecules on the carbon steel surface. It covers the carbon steel surface by reducing both cathodic and anodic reactions. It has been observed that the corrosion *IE* of ANPT can be further improved to 70 % by adding a low concentration of surfactant cetyltrimethyl ammonium bromide. The results of this study are expected to widen the application of thiadiazole derivatives for corrosion inhibition.

# **1. CHAPTER INTRODUCTION**



## 1.1 General Introduction

Metal corrosion is a well-known topic that destroys almost 3% of the world's gross domestic product [1]. It has become a global problem that needs to be lessened. Generally, the corrosion rate (*CR*) depends on two major factors: (a) the nature of the metal and (b) the corrosion media [2]. Due to their unique mechanical properties, metals like low-cost carbon steel (CS) are the most preferred constructive material widely used in industries such as reinforced concrete, oil and gas field, and automobiles [3-5]. But CS is generally susceptible to corrosion under industrial operations such as using mineral acids (HCl, H<sub>2</sub>SO<sub>4</sub>, HNO<sub>3</sub>, etc.) [6]. Among them, hydrochloric acid (HCl) is used on a large scale in industrial applications such as the production of vinyl chloride, hydrometallurgical processing, chlorine dioxide synthesis, hydrogen production, activation of petroleum wells, miscellaneous cleaning, metal cleaning (*e.g.* steel pickling) and so on [7]. During all these processes, this acid becomes an extensive corrosive media for CS [8]. To deal with this problem, several types of the phenomenon are commonly practiced to reduce this material loss, such as coating, cathodic and anodic preventions, metal selection, corrosion inhibitors, and design improvement [2]. However, in most cases, these techniques are complex and require great human effort [9]. Usually, corrosion inhibitors are used as suitable alternatives to reduce this material loss in corrosive media [10-11]. Applying inorganic and organic compounds as corrosion inhibitors (CI) are preferable due to their high efficiency and cost-effectivity, especially in industries [12-13]. Generally, organic corrosion inhibitors are adsorbed on the metal surface through physical or chemical bonds, making a barrier between the surface and corrosive media and protecting the metal from corrosion [14-15]. Thiadiazole derivatives have gained enormous attention as corrosion inhibitors due to its remarkable performance in various aggressive media. Based on the aqueous environment's non-toxicity and stability, the thiadiazole derivative is a good choice for inhibition [16-18]. Furthermore, the presence of a heterocyclic ring of polar amine group along with nitrogen and sulfur atoms and the nitro group in the structure enhances the corrosion Inhibition efficiency (*IE*) compared with those containing only one atom or group among them (**Figure 1. 1**) [19-22].

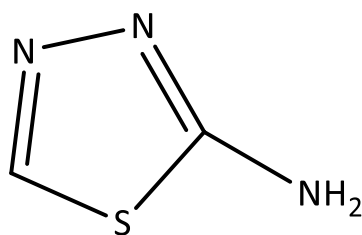


**Figure 1. 1** The chemical structure of 2-amino-1,3,4-thiadiazole

These aforementioned characteristics of thiadiazole derivatives are pointing to being efficient corrosion inhibitors with the desired IE to protect carbon steel in corrosive media. The selected thiadiazole derivative 2-amino-5-(4-nitrophenyl)-1,3,4-thiadiazole (ANPT) with all these properties is supposed to be good corrosion inhibitor. Furthermore, surfactants are also used as corrosion inhibitors [23-24]. The addition of surfactant shows a remarkable change in the IE of thiadiazole [25].

## 1.2 The objective of this work

This work aims to investigate the corrosion inhibition properties of ANPT over CS. The specific objectives of this work are to

- I. synthesize ANPT
- II. investigate ANPT as a corrosion inhibitor
- III. observe the change in IE after adding surfactant
- IV. comprehend the inhibition mechanism through the experimental data obtained

## 1.3 Carbon Steel

CS is an alloy of iron and carbon, whereas the percentage of carbon content isn't more than 2.11 wt. % along with phosphorus, sulfur, and manganese at a minimal amount. The portion of carbon content influences the properties of CS, such as hardness and strength. CS is harder than wrought iron, malleable and flexible, unlike cast iron. Depending on carbon content, CS is primarily classified into three classes. They are- (a) low CS, (b) medium CS and (c) high CS [26].

The presence of carbon in CS increases the hardness and wear resistance of the alloy. CS containing 0.25 % to 0.30 % carbon is known as Low CS [27]. They are relatively soft and weak, possessing excellent ductility and toughness. They are susceptible to damage in corrosive media. Low CS is the most used CS today due to its machinability, weldability, and cost-friendliness compared to other steels. Medium CS contains carbon in a range of 0.30 % – 0.55 % conducting high mechanical properties [27]. They have low hardenability and can be used without heat treatment for some applications. Compared to low CS, medium CS has lower ductility and toughness. They are used mainly in tempered conditions and have a tempered microstructure. High CS has a limited application due to its higher production cost, poor ductility, and weldability. They are usually used in hardened and tempered conditions. The carbon content of High CS is around 0.55 % - 1.00 % [27-28]. Besides these three types of CS, there is also one type of CS called Ultra-high CS containing 1.00 % to 2.10 % carbon. Due to its unique mechanical properties, it can be strong and ductile at room temperature [27, 29].

#### **1.4 Corrosion**

Corrosion can be described as the destruction or deterioration of metals by their surroundings. This is a damaging process of the metals or alloys in contact with corrosive media [30]. Through this process, the metals lose their characteristics. In another way, corrosion is an electrochemical process in aqueous media [31-32].

#### **1.5 Economic Aspects of Corrosion**

Corrosion causes substantial economic losses by severely degrading material properties [33]. This became a global issue due to its direct and indirect financial loss. The international expense of corrosion is supposed to be \$ 2.5 trillion, equivalent to 3.4 % of the global GDP (2013) [10]. This expenditure can be lessened by up to 15 % to 30 % by practicing corrosion control techniques or methods [34]. The corrosion problem in Bangladesh is more severe due to its humid weather than in any other cold and developed country. The increased humidity in the air is more favorable for corrosion reactions. Moreover, a lack of public awareness also worsens this situation [35].

## 1.6 Types of Corrosion

Corrosion is generally identified as rust formation on the metal surface. Corrosion in an aqueous medium is an electrochemical process [32]. Generally, corrosion is the degradation of metals in corrosive media. Based on nature and environment, corrosion can be classified into various forms. They are briefly described below:

### 1.6.1 General Corrosion

General corrosion, also named uniform corrosion, is the simplest form. This corrosion does not penetrate very deep inside the metal. Generally, metal loss on the surface due to a chemical attack or dissolution of the metallic component is defined as general corrosion. Iron rusting, tarnishing silver, and fogging of nickel are examples of general corrosion [31].

### 1.6.2 Pitting Corrosion

Pitting corrosion is occurred due to localized attacks causing cavities or pits on the metal surface. In **Figure 1. 2** a schematic diagram of pitting corrosion is shown. This type of corrosion by itself is a corrosion mechanism. The rate of pitting corrosion on the surface is not uniform, resulting in cavities being more significant in some areas than in others [31]. The shape of the pits differs from each other despite being on the same surface. Metals having films on the surface are more susceptible to this corrosion. The pitting decay generally proceeds through the breakdown of the protective film on the surface. With time the depth of the pits can increase [36]. For example, in soil, the buried iron got shallow pits on its surface, whereas deep holes are observed on stainless steel when immersed in seawater.

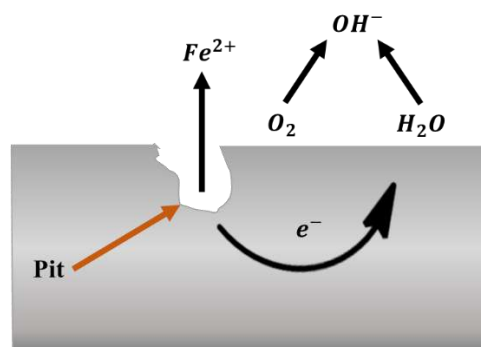


**Figure 1. 2** Pitting corrosion on CS

### 1.6.3 Dealloying, Dezincification and Parting

Dealloying refers to the selective metal corrosion of an alloy [32]. For example, in brass (zinc alloy), the removal of zinc through corrosion. This is known as dezincification. Parting defines as the removal of one or more components preferentially by corrosion. This is similar to dezincification [31].

### 1.6.4 Intergranular Corrosion

Intergranular corrosion is defined as the localized attack on the grain boundaries of the metal or alloy resulting in loss of ductility and strength [37]. For instance, on heating to a temperature of 950 – 1450 °F the stainless steel fails due to intergranular corrosion.

### 1.6.5 Stress-Corrosion Cracking

Stress-corrosion cracking refers to the delayed failure of alloy or metal by cracking. This happens due to continuous exposure of the metal surface in the corrosive environment and static tensile stress [31]. For example, structural metals are susceptible to stress-corrosion cracking.

### 1.6.6. Galvanic Corrosion

Galvanic corrosion occurs in a corrosive electrolyte immersing two connected dissimilar metals with potential differences. When two metals with different potentials are connected in an electrolyte, the galvanic cell is named. Due to potential differences between the metals, electron flow exists between them. In the cell, a metal with a higher *CR* is the anode; the other is the cathode. In short, the potential difference is the driving force of galvanic corrosion [37]. For example, the corrosion of CS in a galvanic cell is caused by coupling CS to copper [32].

### 1.6.7 Crevice Corrosion

Crevice corrosion occurs on the metal surface due to the deposition of dirt, dust, and mud on the surface or by crevices, cavities, and other defects in corrosive media. This is a localized type of corrosion formed by metal-to-metal or metal-to-nonmetal contact [37]. For example, stainless steel undergoes crevice corrosion in a chloride environment by forming ferric or ferrous chloride in the crevices [32].

### 1.6.8 Corrosion Fatigue

Corrosion fatigue refers to metal fractures by fatigue prematurely under the combined attack of corrosive media and cyclic or fluctuating stress [36]. For example, this type of corrosion is usually found in ships, aircraft, heat exchanger tubes, pump shafts and steam turbine blades [37].

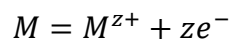
### 1.6.9 Fretting Corrosion

Fretting corrosion occurs when the cyclic relative motion between two adjacent metal surfaces is restricted to a very small amplitude of vibration [37]. This type of corrosion is a combination of wear and corrosion. For say, a stainless-steel spacer used to install a control rudder on the space shuttle exhibits fretting. Fretting corrosion also affects the bolted fish plates used in railroad tracks and causes wheels and turbines to become detached from their mounting shafts [32].

## 1.7 Electrochemical Principles of Corrosion

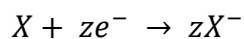
Corrosion is the process through which it returns to its thermodynamic condition. Metals form the metal oxides or sulfides after corrosion as they are collected from the ores. This process proceeds through an electrochemical reaction [38].

In aqueous media, corrosion frequently takes place by forming short-circuited galvanic cells. Some sites of metal surface act as an anode, facilitating oxidation at these sites.

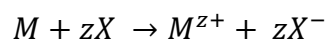


where, z is a stable valance of a given metal, M.

Electrons generated from the anode flow to the cathode are consumed by the cathodic sites by reduction reaction.

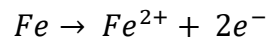


Thus the overall reaction is,

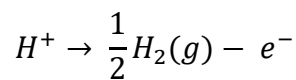


These reactions are spontaneous and result in the loss of metal.

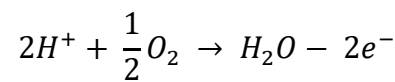
The rust formation on the CS surface is also an electrochemical process, whereas, at the anodic area, the following reaction takes place:



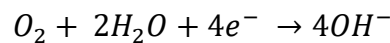
Through this oxidation reaction, the anode produces some current. The cathodic reaction controls the rate of this reaction or the *CR* of iron. In a deaerated solution, the most common response is hydrogen reduction. The reaction is rapid in an acid environment and slower in alkaline or neutral media. The following hydrogen reduction reaction generates hydrogen gas.



Dissolved oxygen can accelerate the cathodic process called depolarization [36]. The reaction is given below:

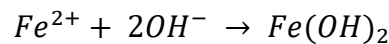


The  $O_2$  reduction involves the conversion of dissolved  $O_2$  gas to hydroxyl ions ( $OH^{-}$ ), the overall reaction is:

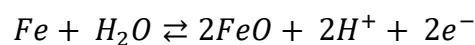


A common pathway for this  $4e^{-}$  process is through the formation of hydrogen peroxide.

In a stable alkaline medium, ferrous hydroxide  $Fe(OH)_2$  was generated due to the secondary reaction between  $Fe^{2+}$  and  $OH^{-}$ .

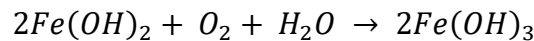


$Fe(OH)_2$  is water-insoluble and commonly known as rust. Another equilibrium reaction also takes place between iron and water mentioned below:

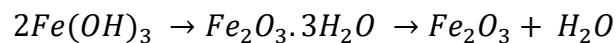
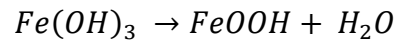


Forms a monolayer of FeO islands [37].

In the presence of  $O_2$ ,  $Fe(OH)_2$  could oxidize to ferric hydroxide  $Fe(OH)_3$  which has very low solubility



The pH of saturated  $Fe(OH)_3$  is almost neutral.  $Fe(OH)_3$  is unstable and could be converted into more stable products.



Between hydrous  $Fe_2O_3$  and  $FeO$ , a dark intermediate layer frequently occurs that is composed of a magnetic hydrous ferrous ferrite,  $Fe_3O_4 \cdot nH_2O$ . So, in most cases, three layers of iron oxides in varying degrees of oxidation make up rust films [31]. The process of rust formation on CS in the presence of air and water has been shown in **Figure 1. 3**.

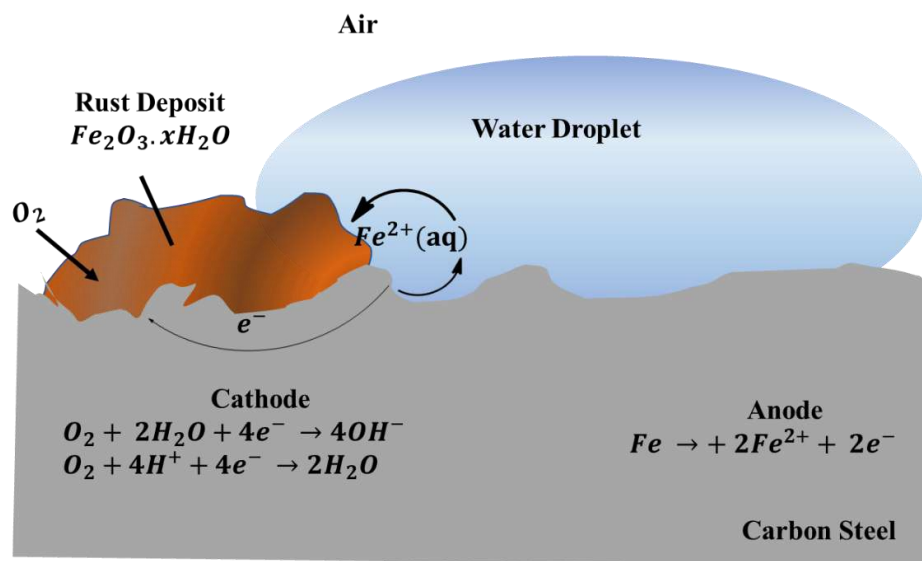


**Figure 1. 3** Rust formation on CS in the presence of water and air

### 1.8 Corrosion Inhibitors

Corrosion inhibitors (CI) are chemical substances that suppress metal corrosion. They can reduce  $CR$  through low consumption [39]. In the beginning, the Romans used bitumen and tar to preserve iron. Some of the foundations of corrosion were recognized shortly after discovering the galvanic cell and the link between electricity and chemical



changes. Throughout the nineteenth century, inhibitors like glue, gelatin, bran, and vegetable oils were employed to prevent iron corrosion in acids [32]. Till now, massive research has been conducted on CI. In the year 2021, Khadim et. al. summarized various works on CIs on different metals or alloys in various environments. They concluded that the inhibition rate can reach around 80 % by using appropriate CI [40]. In Tang's work, an overview of the chemistry, rust inhibition capabilities, and development of CIs for rust-preventative fluids can be found [41]. Based on their solubility and dispersity, CIs are selected for metals or alloys in different corrosive environments. They can be applied either in solid, liquid, or gaseous form. Generally, the inhibition mechanism of the inhibitors proceeds through the adsorption on the metal or alloy surface [42].

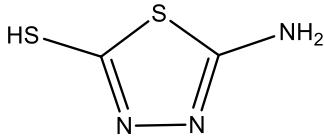
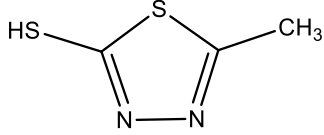
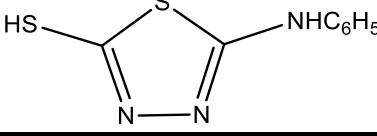
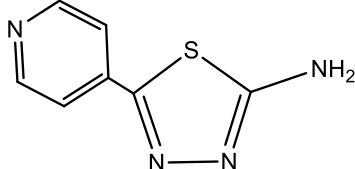
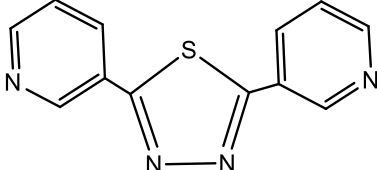
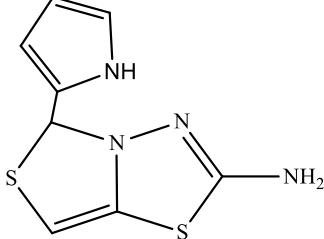
### 1.9 Thiadiazole Derivatives

Thiadiazoles, the hetero-organic compounds, are used as anti-microbial agents or drugs [43]. But for the nontoxicity character, they are widely used as green CI [9, 44]. The cyclic skeleton of the five-membered heterocycle thiadiazole has one sulfur atom, two nitrogen atoms, and two nitrogen atoms. It is discovered that the hetero atom-containing inhibitors have a great capacity to donate electrons, and their efficacy of inhibition rises in the order  $O < N < S$  [13]. In this regard, thiadiazole derivatives are supposed to be efficient inhibitors for CS.

Various research has been conducted on the *IE* of thiadiazole derivatives. For instant, 5-amino 1,3,4-thiadiazole-2-thiol has been reported as an effective inhibitor against 1 M HCl medium, and its efficiency is proportional to its concentration [16]. It's also been found that 2-mercapto-5-amino-1,3,4-thiadiazole (MAT), 2-mercapto-5-acetylamino-1,3,4-thiadiazole, 2-mercapto-5-methyl-1,3,4-thiadiazole and 2-mercapto-5-phenylamino-1,3,4-thiadiazole are efficient CI for bronze against a mixture of  $\text{Na}_2\text{SO}_4$  and  $\text{NaHCO}_3$  solution at pH 5 [17]. Besides, it's also reported that 2-amino-5-(4-pyridinyl)-1,3,4-thiadiazole has high *IE* on the upper surface in 0.1M KCl solution [45]. The 2,5-bis(*n*-pyridyl)-1,3,4-thiadiazoles shows good efficiency as CI in various acidic media such as 1M HCl, 0.5M  $\text{H}_2\text{SO}_4$ , and 1M  $\text{HClO}_4$ . The inhibiting protection depends on the position of the nitrogen on the pyridinium substituent [46]. Furthermore, density functional theory (DFT) was used to successfully determine the geometries of the 2-amino-1,3,4-thiadiazole and its 5-alkyl derivatives and to show how well these

compounds worked as CI of mild steel in 1M H<sub>2</sub>SO<sub>4</sub> [47]. A comparative study of corrosion *IE* of phenyl-substituted amino thiadiazoles such as 5-phenyl-2-amino-1,3,4-thiadiazole (APT) and 5-(4-methoxyphenyl)-2-amino-1,3,4-thiadiazole (AMPT) on copper in 0.5M H<sub>2</sub>SO<sub>4</sub> solution has been performed [48]. When thiazolo thiadiazole (TT) derivatives were tested for their ability to prevent mild steel corrosion in 1M H<sub>2</sub>SO<sub>4</sub>, the results revealed that the effectiveness of the inhibitors increased with increasing inhibitor concentration [49]. In the following **Table 1. 1** the *IE* of some thiadiazole derivatives as corrosion inhibitors are presented.

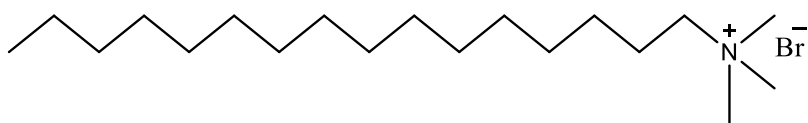
**Table 1. 1** Structure of some developed thiadiazole derivatives as corrossions inhibitor

SI NO.	Name of Thiadiazole derivatives	Structure of Thiadiazole derivatives	<i>IE</i>	Ref.
1	5-amino 1,3,4-thiadiazole-2-thiol (5-ATT)		90 %	[16]
2	2-mercapto-5-methyl-1,3,4-thiadiazole (MMeT)		90 %	[17]
3	2-mercapto-5-phenylamino-1,3,4-thiadiazole (MPhAT)		90 %	[17]
4	2-amino-5-(4-pyridinyl)-1,3,4-thiadiazole (4-APTD)		90 %	[45]
5	2,5-bis-(3-pyridyl)-1,3,4-thiadiazole (3-PTH)		Around 90 %	[46]
6	5-(4-methoxyphenyl)-2-amino-1,3,4-thiadiazole (AMPT)		97 %	[49]

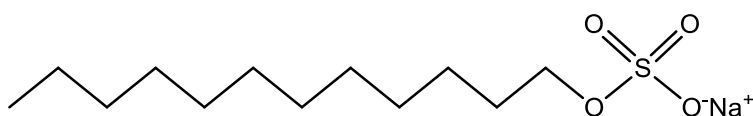
## 1.10 Synergistic Effect on Organic Corrosion Inhibitors

The interaction of two or more substances, agents, entities, or factors results in a synergistic effect, an effect that is greater than the sum of its parts. This is a helpful method for increasing the inhibitors' ability to inhibit, reducing their consumption, and diversifying their uses in acidic media [50]. Numerous research had clarified the function of synergism in the corrosion prevention mechanism of mild steel in acidic media [51-52]. A few studies focused on the interaction of surfactants with various chemical molecules [53-54]. Surfactants or surface-active compounds decrease the interfacial tension or interfacial free energy of the interfaces and contain a hydrophilic region along with the hydrophobic part. The synergistic effect caused by the addition of surfactant increases the *IE* of thiadiazole derivatives for mild steels in an acidic medium [25]. **Figure 1. 4** represents some structures of surfactants. There are four types of surfactants. They are:

- (a) cationic surfactant (examples of some common cationic surfactants include alkyl ammonium chlorides)
- (b) anionic surfactant (sulfates, sulfonates, and gluconates are examples of anionic surfactants)
- (c) nonionic surfactant (examples of some common nonionic surfactants include cocamide, ethoxylates, and alkoxyates)
- (d) amphoteric surfactant (examples of some frequently used amphoteric surfactants are betaines and amino oxides).



(a) Cetyl-*N, N, N*-trimethyl ammonium bromide (CTAB)



(b) Sodium dodecyl sulfate (SDS)

**Figure 1. 4** Structures of surfactants, (a) CTAB and (b) SDS.

### 1.11 Adsorption Phenomenon of CI on Metal Surface

Generally speaking, adsorption is thought to be the initial step in the acid inhibition process. The type of aggressive medium, the inhibitor's chemical nature and the composition and surface charge of metals have an impact on adsorption [55]. There are two types of adsorption, such as (a) physical adsorption and (b) chemisorption. The inhibitor molecules' electrostatic attraction to the electrical charge on the metal surface leads to electrostatic adsorption. But, in chemisorption, inhibitor molecules, and metal surfaces have already formed a coordination bond exchange or share charges [56]. Besides these two types of adsorption, surface interaction between the inhibitor molecules also causes strong adsorption [57].

### 1.12 Theories of Experimental Techniques

Various techniques have been developed for determining metal *CR* (*CR*) and *CI*'s *IE*. For say, weight-loss measurements, scanning electron microscopy (SEM) for surface analysis, adsorption isotherms & thermodynamic characterization, and electrochemical techniques are familiar names in the field of corrosion science.

### 1.13 Weight-loss Measurement

Weight-loss measurement (WL) is one of the most reliable techniques for the determination of *CR* and *IE*. This quantitative technique is used to measure and analyze metals' internal or exterior corrosion. In this technique, the weight of the metal is measured in the corrosive medium at periodic intervals. Since just time (*t*) and weight (*W*) is involved, which are simple indices to get, this corrosion monitoring method may be the simplest. It determines the corrosion type in a particular environment and the appropriateness of various design materials.

Usually, coupons are used in weight loss analysis and characterization. The technique involves placing the coupons in a particular setting, removing the samples after a predetermined time, cleaning them for net weight, and monitoring the weight difference ( $\Delta W$ ) by periodic intervals. The recorded data from this technique is used in a known engineering formula leading to the calculation of the *CR*. If *A* is the surface area of the specimen, then the equation of the *CR* determination is

$$CR (mg.cm^{-2}.h^{-1}) = \frac{\Delta W}{A \times t} \quad (1)$$

The  $IE_{WL}$  and surface coverage ( $\theta$ ) can be calculated from the following equations,

$$IE_{WL} \% = \frac{CR_0 - CR_{inh}}{CR_0} \times 100 \quad (2)$$

$$\theta = \frac{IE_{WL}}{100} \quad (3)$$

Where  $\Delta W$  is the weight loss in mg,  $A$  is the exposed surface area in  $cm^2$  in solution,  $t$  is the exposure time in hours, and  $CR_0$  and  $CR_{inh}$  are respectively the  $CR$  in uninhibited and inhibited corrosive solution [53].

#### 1.14 Scanning Electron Microscopy (SEM)

A sophisticated technique used to photograph the microstructure of the materials is Scanning Electron Microscopy (SEM). SEM is typically performed in a high vacuum because gas molecules tend to disturb the electron beam and the emitted secondary and backscattered electrons used for imaging. Before the morphological inspection, the specimen is reduced in size and coated with aurum [58]. A light microscope can typically magnify images up to 1000 to resolve details down to  $0.2 \mu m$  [59]. Similarly, electron beam interaction with the specimen emits an energy-dispersive X-ray (EDX) with a unique energy that can be detected to determine the composition of the material under examination [59].

#### 1.15 Adsorption Isotherm and Thermodynamic Characterization

Adsorption isotherm provides a better understanding of the mechanism of CI on the metal surface. The adsorption isotherm describes the interaction of the inhibitor molecule with the metal surface [60]. Several adsorption isotherms, including Temkin, Freundlich, and Langmuir adsorption isotherms, are used to understand the interaction mechanism between CI and the metal surface [20].

According to the above adsorption isotherms, surface coverage ( $\theta$ ) is related to inhibitors' concentration ( $C$ ). Then the adsorption models' formulae are as follows:

Langmuir :

$$\frac{\theta}{(1-\theta)} = K_{ads}C_{inh} \quad (4)$$

Freundlich: 
$$\log \theta = \log K_{ads} + \frac{1}{n} \log C_{inh} \quad (5)$$

Temkin: 
$$\theta = \ln C_{inh} + K_{ads} \quad (6)$$

Frumkin: 
$$\log \frac{\theta}{(1-\theta)C_{inh}} = \log K_{ads} + g\theta \quad (7)$$

Where,

$K_{ads}$  is the adsorption equilibrium constant,

$C_{inh}$  is the inhibitor concentration,

$g$  is the adsorbate interaction parameter,

$n$  is the constant at any temperature.

The above adsorption isotherms are all tested to fit the experimental data. However, which one provides the best linear fits with the correlation coefficient ( $r^2$ ) > 0.9 is finally chosen for further study of the corrosion inhibition mechanism of inhibitors. If a graph of  $C_{inh}$  vs  $C_{inh}/\theta$  is plotted, then  $K_{ads}$  is calculated from the intercept. Using the following equation, standard free energy can be calculated:

$$\Delta G_{ads}^0 = -RT \ln(55.5 K_{ads}) \quad (8)$$

Where  $R$  is the universal gas constant, and  $T$  is the absolute temperature and the constant value, 55.5 represents the molar concentration of water in solution. The negative value of  $\Delta G_{ads}^0$  indicates the spontaneity of the reaction. The adsorption will be non-spontaneous for the value positive value of Gibb's free energy [16, 20, 60].

### 1.16 Thermodynamic Parameters

The temperature has a significant effect on adsorption, and using the  $CR$  and  $IE$  at different temperatures, activation energy ( $E_a$ ), activation enthalpy ( $\Delta H_a^0$ ) and activation entropy ( $\Delta S_a^0$ ) can be calculated [60]. The following Arrhenius-type equation may be used to estimate the computed values of apparent activation energy ( $E_a$ ) for the corrosion process:

$$\ln(CR) = -\frac{E_a}{RT} + A \quad (9)$$

$R$  is the general gas constant,  $T$  is the absolute temperature, and  $A$  is the Arrhenius pre-exponential factor [16].

However, the activation enthalpy ( $\Delta H_a^0$ ) and activation entropy ( $\Delta S_a^0$ ) can be calculated from the following alternative Arrhenius equation:

$$CR = \frac{RT}{Nh} \exp\left(\frac{\Delta S_a^0}{R}\right) \exp\left(-\frac{\Delta H_a^0}{RT}\right) \quad (10)$$

Where,  $h$  is Plank's constant and  $N$  is Avogadro's number [16, 61].

Equation (10) can be rewritten in the following form,

$$\ln\left(\frac{CR}{T}\right) = -\frac{\Delta H_a^0}{R} \times \frac{1}{T} + \ln\left(\frac{R}{Nh}\right) + \left(\frac{\Delta S_a^0}{R}\right) \quad (11)$$

Here,  $\Delta H_a^0$  can be calculated from the slope  $-\frac{\Delta H_a^0}{R}$  of the plot  $\frac{CR}{T}$  against  $\frac{1}{T}$  and  $\Delta S_a^0$  can be calculated from the intercept of  $\ln\left(\frac{R}{Nh}\right) + \left(\frac{\Delta S_a^0}{R}\right)$  [60].

## 1.16 Electrochemical Techniques

Electrochemical techniques give an electrical component that enables the measurement of corrosion currents. These currents estimate the  $CR$ s that may be used to predict equipment and structural service lifespan [64]. The following techniques are generally used to estimate the metal and metal alloy  $CR$ s:

### 1.16.1 Open Circuit Potential

Open circuit potential (OCP) or corrosion potential are the terms used to describe electrode potential when no applied voltage is present. OCP is the potential measured between the working electrode (WE) and the reference electrode (RE) in the absence of current[62].

When the WE is immersed in the aqueous corrosive media, one type of layer is formed on it consisting of (a) the negative charge of the valance electron of the surface atom, (b) adsorbed water molecule, and (c) the positively charged metal ions. This layer is mentioned as an electrical double layer (EDL) [62]. In **Figure 1. 5** a schematic diagram of EDL has been represented.

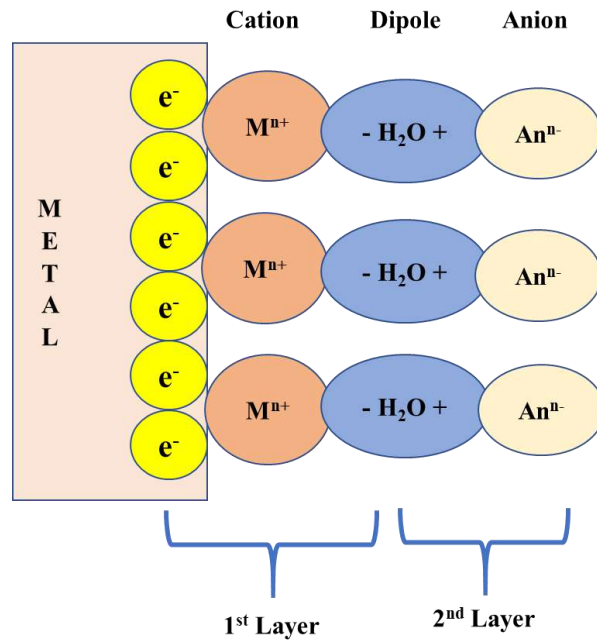


**Figure 1. 5** EDL

The EDL's charge separation produces an electrical potential that can be measured as the difference between two metal electrodes or a metal and reference electrode [62]. This electrical potential is OCP, represented as a time vs potential graph shown in **Figure 1. 6**. It is possible to determine the corrosion in a specific metal environment by measuring WE OCP.

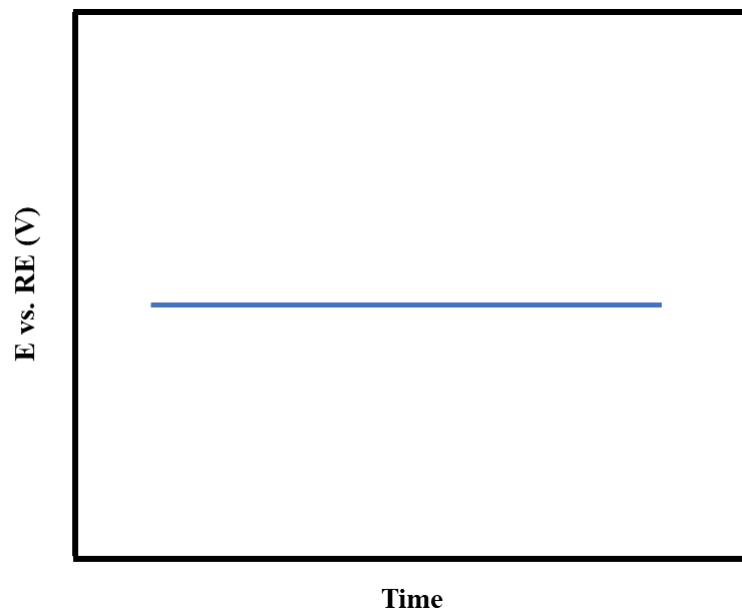


**Figure 1. 6** Schematic diagram of OCP plot



### 1.16.2 Potentiodynamic Polarization

Potentiodynamic polarization (PDP) is a technique where the electrode's potential is varied at a selected rate by applying a current through the electrolyte. The PDP method is used to identify the potential area at which an alloy or metal becomes passive when exposed to a particular environment. This method estimates the information about the  $CR$ , passivity, and cathodic behavior of an electrochemical system [63]. In this technique, the potential of a sample is scanned or stepped in small increments over a range from below the corrosion potential or OCP to well above the OCP. The current passed at the electrode surface is determined as a function of the potential. The current density is easily calculated and is often plotted as a function of potential on a semi-log plot. Such a plot is called a polarization curve [64].

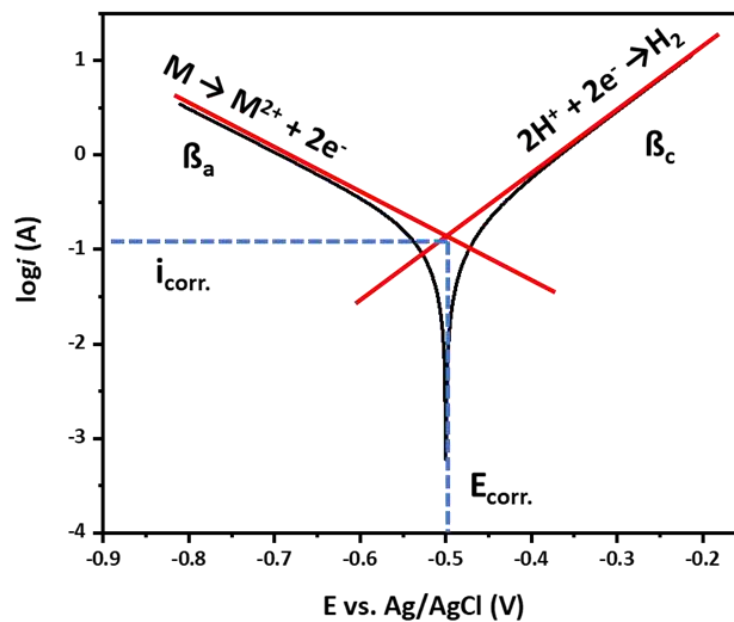


**Figure 1. 7** Schematic diagram of Tafel plot

In the polarization curve, the absolute value of the current is plotted, as the log of a negative number is undefined. The relationship tends to follow the straight-line characteristic of Tafel kinetics for the anodic reaction ( $\beta_a$ ) at high potentials and the cathodic reaction ( $\beta_c$ ) at low potentials because one of the processes, either the cathodic or anodic reaction, occurs at a significantly larger rate far from the corrosion potential. In the plot, the potential at which the curve points is called corrosion potential ( $E_{corr.}$ )

where the anodic current is equal to the cathodic current. Moreover, the extrapolation of the anodic reaction and cathodic reaction to the corrosion potential gives an intersection of anodic and cathodic Tafel lines [64]. This intersection point is termed the corrosion current ( $i_{corr}$ ). A Tafel plot has been shown in **Figure 1. 7**. By using this corrosion current the  $CR$  and  $IE_{PDP}$  can be calculated from the following equation:

$$IE_{PDP} \% = \frac{i_{corr} - i_{inh}}{i_{corr}} \times 100 \quad (12)$$

where,  $i_{corr}$  and  $i_{inh}$  are the corrosion current densities of solution without or with inhibitors, respectively [16,19].

### 1.16.3 Electrochemical Impedance Spectroscopy

Electrochemical impedance spectroscopy (EIS) demonstrates how surface inhomogeneities impact corrosion processes [65]. This is a widely practiced corrosion science technique [17, 24, 45]. EIS perturbs an electrode surface with brief periodic signals, measuring the electrochemical response that may be examined to learn more about corrosion kinetics and processes. In corrosion investigations, a 10 to 50 mV sinusoidal voltage signal is frequently applied to a corroding electrode interface, and the subsequent current signal is measured at the same excitation frequency. Impedance is measured over a range of distinct frequencies from 100 MHz to 100 KHz, making the measurement spectroscopic [66]. An electronic circuit known as the equivalent electrical circuit of capacitors and resistors is used in EIS to represent the corrosion cell or any electrochemical discharge reaction at the electrode interface. This type of circuit usually consists of solution resistance ( $R_s$ ), double layer capacitance ( $C_{dl}$ ) and charge transfer resistance ( $R_{ct}$ ) [63].

In corrosion studies, EIS data are graphically presented in Nyquist and Bode plots. A simple circuit and a schematic diagram of Nyquist plot and Bode plot are shown in **Figure 1. 8**. In Nyquist plot, the impedance at each frequency is located according to its real and imaginary components. At each frequency, the magnitude of this impedance is equal to the length of the vector drawn to the point from the plot origin. In Bode plots, the log of the impedance magnitude and the phase angle is plotted versus the logarithm of the applied frequency. The impedance is primarily resistive at the highest and lowest frequencies, and the Bode magnitude plots are flat [66].

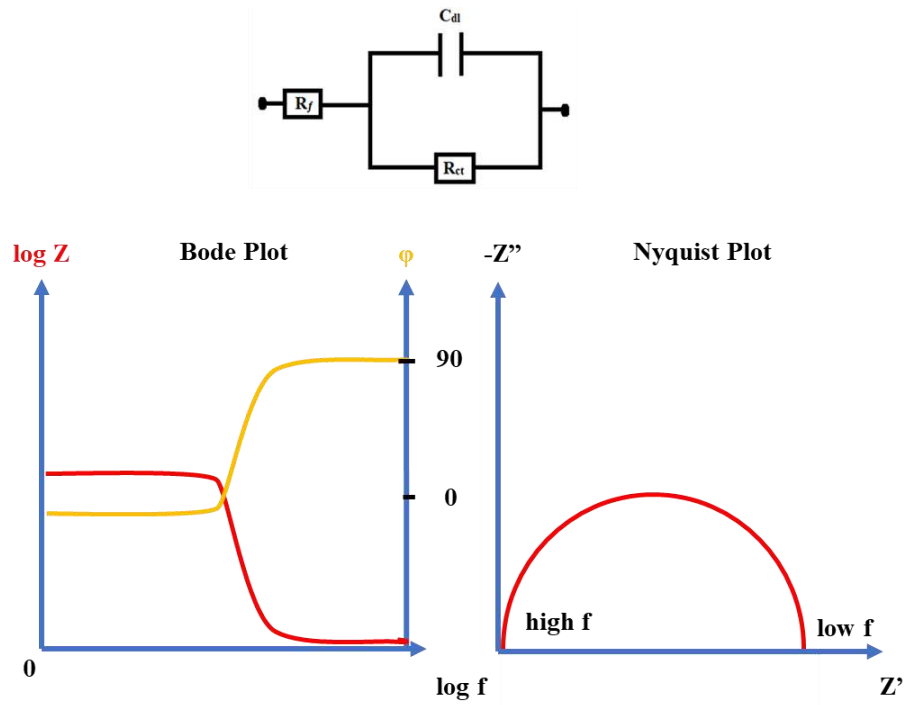


**Figure 1. 8** Schematic diagram of Nyquist plot and Bode plot

Nyquist and Bode plots are used to obtain information about the  $CR$  and  $IE_{EIS}$ . The EIS experiments are performed with an amplitude signal frequency range. The  $IE_{EIS}$  is analyzed by the EIS technique through the following equation:

$$IE_{EIS} \% = \frac{R_{ct(inh)} - R_{ct}}{R_{ct(inh)}} \times 100 \quad (12)$$

Where,  $R_{ct}$  and  $R_{ct(inh)}$  are the charge transfer resistances without or with inhibitors for WE in an aqueous solution, respectively [17].

## References

- [01] F. U. Renner, A. Stierle, H. Dosch, D. M. Kolb, T. L. Lee, and J. Zegenhagen, "Initial corrosion observed on the atomic scale," *Nature*, vol. 439, pp. 707–710, 2006.
- [02] S. A. Umoren and M. M. Solomon, "Protective polymeric films for industrial substrates: A critical review on past and recent applications with conducting polymers and polymer composites/nanocomposites," *Prog. Mater. Sci.*, vol. 104, pp. 380–450, 2019.
- [03] N. R. Baddoo, "Stainless steel in construction: A review of research, applications, challenges and opportunities," *J. Constr. Steel Res.*, vol. 64, pp. 1199–1206, 2008.
- [04] K. A. Cashell and N. R. Baddoo, "Ferritic stainless steels in structural applications," *Thin-Walled Struct.*, vol. 83, pp. 169–181, 2014.
- [05] Q. Chen, K. Finney, H. Li, X. Zhang, J. Zhou, V. Sharifi and J. Swithenbank, "Condensing boiler applications in the process industry," *Appl. Energy*, vol. 89, pp. 30–36, 2012.
- [06] V. Sudarsan, "Materials for Hostile Chemical Environments," in *Materials Under Extreme Conditions: Recent Trends and Future Prospects*, Elsevier Sci., pp. 129–158, 2017.
- [07] J. G. Speight, "Industrial Inorganic Chemistry," in *Environmental Inorganic Chemistry for Engineers*, Elsevier Sci., pp. 111–169, 2017.
- [08] E. A. Noor, A. Al-Moubaraki, and A. H. Al-Moubaraki, "Corrosion Behavior of Mild Steel in Hydrochloric Acid Solutions Comparative studies of corrosion behavior and corrosion inhibition for selected metals in water wood extract View project Corrosion Behavior of Mild Steel in Hydrochloric Acid Solutions," *Int. J. Electrochem. Sci.*, vol. 3, pp. 806 – 818, 2008.
- [09] C. Verma, M. A. Quraishi, and K. Y. Rhee, "Present and emerging trends in using pharmaceutically active compounds as aqueous phase corrosion inhibitors," *J. Mol. Liq.*, vol. 328, 115395, 2021.
- [10] D. Dwivedi, K. Lepková, and T. Becker, "Carbon steel corrosion: a review of key surface properties and characterization methods," *RSC Adv.*, vol. 7, pp. 4580–4610, 2017 .
- [11] T. G. Harvey, S.G. Hardin, A.E. Hughes, T.H. Muster, P.A. White, T.A. Markley, P.A. Corrigan, J. Mardel, S.J. Garcia, J.M.C. Mol and A.M. Glenn, "The effect of inhibitor structure on the corrosion of AA2024 and AA7075," *Corros. Sci.*, vol. 53, pp. 2184–2190, 2011.
- [12] M. A. Quraishi, D. S. Chauhan, and V. S. Saji, "Heterocyclic biomolecules as green corrosion inhibitors," *J. Mol. Liq.*, vol. 341, pp. 117265, 2021.
- [13] L. Guo, I.B. Obot, X. Zheng, X. Shen, Y. Qiang, S. Kaya and C. Kaya, "Theoretical insight into an empirical rule about organic corrosion inhibitors containing nitrogen, oxygen, and sulfur atoms," *Appl. Surf. Sci.*, vol. 406, pp. 301–306, 2017.

- [14] T. J. Harvey, F. C. Walsh, and A. H. Nahlé, “A review of inhibitors for the corrosion of transition metals in aqueous acids,” *J. Mol. Liq.*, vol. 266, pp. 160–175, 2018.
- [15] K. Khanari, M. Finšgar, M. Knez Hrnčič, U. Maver, Ž. Knez, and B. Seiti, “Green corrosion inhibitors for aluminium and its alloys: A review,” *RSC Adv.*, vol. 7, pp. 27299–27330, 2017.
- [16] H. Ouici, M. Tourabi, O. Benali, C. Selles, C. nJama, A. Zarrouk and F. Bentiss, “Adsorption and corrosion inhibition properties of 5-amino 1,3,4-thiadiazole-2-thiol on the mild steel in hydrochloric acid medium: Thermodynamic, surface and electrochemical studies,” *J. Electroanal. Chem.*, vol. 803, pp. 125–134, 2017.
- [17] S. Varvara, L. M. Muresan, K. Rahmouni, and H. Takenouti, “Evaluation of some non-toxic thiadiazole derivatives as bronze corrosion inhibitors in aqueous solution,” *Corros. Sci.*, vol. 50, pp. 2596–2604, 2008.
- [18] S. Xue and Z. Xue, “Microwave-assisted one-pot synthesis and performance test of novel thiadiazole derivatives as an inhibitor of oil transportation pipelines,” *Anti-Corros. Methods Mater.*, vol. 64, pp. 461–464, 2017.
- [19] H. J. Habeeb, H. M. Luaibi, R. M. Dakhil, A. A. H. Kadhum, A. A. Al-Amiery, and T. S. Gaaz, “Development of new corrosion inhibitor tested on mild steel supported by electrochemical study,” *Results Phys.*, vol. 8, pp. 1260–1267, 2018.
- [20] M. Palomar-Pardavé, M. Romero-Romo, H. Herrera-Hernández, M.A. Abreu-Quijano, N.V. Likhanova, J. Uruchurtu, and J.M. Juárez-García, “Influence of the alkyl chain length of 2 amino 5 alkyl 1,3,4 thiadiazole compounds on the corrosion inhibition of steel immersed in sulfuric acid solutions,” *Corros. Sci.*, vol. 54, pp. 231–243, 2012.
- [21] B. Chugh, A.K. Singh, S. Thakur, B. Pani, H. Lgaz, I.M. Chung, R. Jha and E.E. Ebenso, “Comparative Investigation of Corrosion-Mitigating Behavior of Thiadiazole-Derived Bis-Schiff Bases for Mild Steel in Acid Medium: Experimental, Theoretical, and Surface Study,” *ACS Omega*, vol. 5, pp. 13503–13520, 2020.
- [22] S. S. Al-Shihry, A. R. Sayed, and H. M. Abd El-lateef, “Design and assessment of a novel poly(urethane-semicarbazides) containing thiadiazoles on the backbone of the polymers as inhibitors for steel pipelines corrosion in CO<sub>2</sub>-saturated oilfield water,” *J. Mol. Struct.*, vol. 1201, pp. 127223, 2020.
- [23] Y. Zhu, M. L. Free, R. Woollam, and W. Durnie, “A review of surfactants as corrosion inhibitors and associated modeling,” *Prog. Mater. Sci.*, vol. 90, pp. 159–223, 2017.
- [24] R. Fuchs-Godec and M. G. Pavlović, “Synergistic effect between non-ionic surfactant and halide ions in the forms of inorganic or organic salts for the corrosion inhibition of stainless-steel X<sub>4</sub>Cr<sub>13</sub> in sulphuric acid,” *Corros. Sci.*, vol. 58, pp. 192–201, 2012.
- [25] J. Saranya, P. Sounthari, A. Zarrouk, S. Chitra, “Synergistic effect of halides and surfactants on the corrosion inhibition of thiazolo thiadiazole derivative for mild steel in acid medium,” *Mor. J. Chem*, vol. 5, pp. 164-176, 2017.

- [26] G. Krauss, "Tempering of martensite in carbon steels," in Phase Transformations in Steels, *Elsevier Sci.*, vol. 2 pp. 126–150, 2012.
- [27] T. Islam and H. M. M. A. Rashed, "Classification and Application of Plain Carbon Steels," in Reference Module in Materials Science and Materials Engineering, *Elsevier Sci.*, vol. 2, pp. 14, 2019.
- [28] G. Aggen *et al.*, "Properties and Selection: Irons, Steels, and High-Performance Alloys," ASM Handbook, *ASM International*, vol. 1, pp. 150-179, 2005.
- [29] O. D. Sherby, 'Damascus Steel Rediscovered', *Trans. Iron Steel Inst. Japan*, vol. 19, pp. 381-390, 1979.
- [30] N. Sato, "Basics of Corrosion Chemistry," Green Corrosion Chemistry and Engineering, *Jon Wiley & Sons, Inc.*, chap. 1, pp.1-32, 2011.
- [31] H. H. Uhlig and R. W. Revie, "Corrosion and corrosion control. An introduction to corrosion science and engineering." *Jon Wiley & Sons, Inc.*, Third Edition, pp. 1-514, 1985.
- [32] V. S. Sastri, "Green corrosion inhibitors: theory and practice.", *Jon Wiley & Sons, Inc.*, pp. 1-305, 2011.
- [33] R. Solmaz, "Investigation of the inhibition effect of 5-((E)-4-phenylbuta-1,3-dienylideneamino)-1,3,4-thiadiazole-2-thiol Schiff base on mild steel corrosion in hydrochloric acid," *Corros. Sci.*, vol. 52, pp. 3321–3330, 2010.
- [34] K. Gerhardus, V. Jeff, T. Neil, M. Oliver, G. Melissa, P. Joe, "International measures of Prevention, Application and Economics of Corrosion Technologies Study", *NACE Int.*, pp. 1-19, 2016.
- [35] T. Manzur, B. Baten, M. J. Hasan, H. Akter, A. Tahsin, and K. M. A. Hossain, "Corrosion behavior of concrete mixes with masonry chips as coarse aggregate," *Constr Build Mater.*, vol. 185, pp. 20–29, 2018.
- [36] P. A. Schweitzer, "CORROSION Fundamentals of Mechanisms, Causes, and Preventative Methods." *CRC Press*, pp. 1-379, 2010.
- [37] Zaki Ahmad, "Principles of Corrosion Engineering and Corrosion Control," *Elsevier Sci.*, pp. 1-646, 2006.
- [38] T. E. Graedel and R. P. Frankenthal, "Corrosion Mechanisms for Iron and Low Alloy Steels Exposed to the Atmosphere," *J. Electrochem.*, vol. 137, pp. 2385–2394, 1990.
- [39] M.G. Fontana, "Corrosion Engineering", *McGraw-Hill.*, Third Edition, pp. 278-315, 1986.
- [40] A. Kadhim, A. A. Al-Amiery, R. Alazawi, M. K. S. Al-Ghezi, and R. H. Abass, "Corrosion inhibitors. A review," *Int. J. Corros. Scale Inhib.*, vol. 10, pp. 54–67, 2021.
- [41] Z. Tang, "A review of corrosion inhibitors for rust preventative fluids," *Curr Opin Solid State Mater Sci .*, vol. 23, pp. 100759, 2019.
- [42] G. Palanisamy, "Corrosion Inhibitors." *Intech Open*, pp. 1-24, 2019.
- [43] Y. Li, J. Geng, Y. Liu, S. Yu, and G. Zhao, "Thiadiazole-a Promising Structure in Medicinal Chemistry," *ChemMedChem*, vol. 8, pp. 27–41, 2013.
- [44] G. Gece, "Drugs: A review of promising novel corrosion inhibitors," *Corros. Sci.*, vol. 53, pp. 3873–3898, 2011.

- [45] Y. C. Pan, Y. Wen, X. Y. Guo, P. Song, S. Shen, Y.P. Du and H. F. Yang, “2-Amino-5-(4-pyridinyl)-1,3,4-thiadiazole monolayers on copper surface: Observation of the relationship between its corrosion inhibition and adsorption structure,” *Corros. Sci.*, vol. 73, pp. 274–280, 2013.
- [46] F. Bentiss, B. Mernari, M. Traisnel, H. Vezin, and M. Lagrenée, “On the relationship between corrosion inhibiting effect and molecular structure of 2,5-bis(n-pyridyl)-1,3,4-thiadiazole derivatives in acidic media: Ac impedance and DFT studies,” *Corros. Sci.*, vol. 53, pp. 487–495, 2011.
- [47] N. A. Wazzan, I. B. Obot, and S. Kaya, “Theoretical modeling and molecular level insights into the corrosion inhibition activity of 2-amino-1,3,4-thiadiazole and its 5-alkyl derivatives,” *J. Mol. Liq.*, vol. 221, pp. 579–602, 2016.
- [48] Y. M. Tang, W. Z. Yang, X. S. Yin, Y. Liu, R. Wan, and J. T. Wang, “Phenyl-substituted amino thiadiazoles as corrosion inhibitors for copper in 0.5 M H<sub>2</sub>SO<sub>4</sub>,” *Mater. Chem. Phys.*, vol. 116, pp. 479–483, 2009.
- [49] J. Saranya, F. Benhiba, N. Anusuya, A. Zarrouk, and S. Chitra, “Thiazolo thiadiazole derivatives as anti-corrosion additives for acid corrosion,” *CDC*, vol. 26, pp. 10035, 2020.
- [50] P. C. Okafor and Y. Zheng, “Synergistic inhibition behaviour of methylbenzyl quaternary imidazoline derivative and iodide ions on mild steel in H<sub>2</sub>SO<sub>4</sub> solutions,” *Corros. Sci.*, vol. 51, pp. 850–859, 2009.
- [51] E. E. Oguzie, C. Unaegbu, C. N. Ogukwe, B. N. Okolue, and A. I. Onuchukwu, “Inhibition of mild steel corrosion in sulphuric acid using indigo dye and synergistic halide additives,” *Mater. Chem. Phys.*, vol. 84, pp. 363–368, 2004.
- [52] E. E. Oguzie, Y. Li, and F. H. Wang, “Corrosion inhibition and adsorption behavior of methionine on mild steel in sulfuric acid and synergistic effect of iodide ion,” *J. Colloid Interface Sci.*, vol. 310, pp. 90–98, 2007.
- [53] M. Z. A. Rafiquee, N. Saxena, S. Khan, and M. A. Quraishi, “Influence of surfactants on the corrosion inhibition behaviour of 2-aminophenyl-5-mercapto-1-oxa-3,4-diazole (AMOD) on mild steel,” *Mater. Chem. Phys.*, vol. 107, pp. 528–533, 2008.
- [54] M. Mobin, M. Parveen, and M. Z. A. Rafiquee, “Synergistic effect of sodium dodecyl sulfate and cetyltrimethyl ammonium bromide on the corrosion inhibition behavior of L-methionine on mild steel in acidic medium,” *Arab. J. Chem.*, vol. 10, pp. S1364–S1372, 2017.
- [55] B. Mernari, H. El Attari, M. Traisnel, F. Bentiss, and M. Lagrenée, “Inhibiting effects of 3,5-bis(n-pyridyl)-4-amino-1,2,4-triazoles on the corrosion for mild steel in 1 M HCl medium,” *Corros. Sci.*, vol. 40, pp. 391–399, 1998.
- [56] J. Aljourani, K. Raeissi, and M. A. Golozar, “Benzimidazole and its derivatives as corrosion inhibitors for mild steel in 1M HCl solution,” *Corros. Sci.*, vol. 51, pp. 1836–1843, 2009.
- [57] N. Hackerman, D. D. Justice, E. Mccafferty, “Homopiperazine as a Corrosion Inhibitor,” *Corros.*, vol. 31, pp. 240–242, 1975.

- [58] W. Zhou, R. P. Apkarian, Z. Lin Wang, and D. Joy, “Fundamentals of Scanning Electron Microscopy,” *Scanning Microscopy for Nanotechnology, Springer Sci. Rev.*, First Edition, pp. 1–40, 2006.
- [59] A. Ul-Hamid, “A Beginners’ Guide to Scanning Electron Microscopy,” *Springer Sci. Rev.*, First Edition, pp. 1-421, 2018.
- [60] I. A. Annon, A.S. Abbas, W.K. Al-Azzawi, M.M. Hanoon, A. Alamiery, W.N.R. Isahak and A.A.H. Kadhum, “Corrosion inhibition of mild steel in hydrochloric acid environment using thiadiazole derivative: Weight loss, thermodynamics, adsorption and computational investigations,” *S. Afr. J. Chem. Eng.*, vol. 41, pp. 244–252, 2022.
- [61] F. Bentiss, M. Lebrini, and M. Lagrenée, “Thermodynamic characterization of metal dissolution and inhibitor adsorption processes in mild steel/2,5-bis(n-thienyl)-1,3,4-thiadiazoles/ hydrochloric acid system,” *Corros. Sci.*, vol. 47, pp. 2915–2931, 2005.
- [62] W. S. Tait, “Electrochemical corrosion basics,” in *Handbook of Environmental Degradation Of Materials: Third Edition, Elsevier Sci.*, pp. 97–115, 2018.
- [63] B. N. Popov, “Corrosion engineering : principles and solved problems,” *Elsevier Sci.*, pp. 181-238, 2015.
- [64] G. S. Frankel, “Fundamentals of corrosion kinetics,” *Springer Ser. Mater. Sci.*, vol. 233, p. 17, 2016.
- [65] K. Jüttner, “Electrochemical impedance spectroscopy (EIS) of corrosion processes on inhomogeneous surfaces,” *Electrochim. Acta*, vol. 35, pp. 1501–1508, 1990.
- [66] R. G. Kelly, J.R. Scully, D.W. Shoesmith and R.G. Buchheit, “Electrochemical techniques in corrosion science and engineering,” *Marcel Dekker Inc.*, 2003.



## **2. CHAPTER EXPERIMENTAL**

## 2.1 Chemicals & Reagents

Analytical-grade chemicals were used directly in this study without further purification. Reagents like sodium hydroxide, hydrochloric acid, and ethanol were collected from Merck, Germany. Other chemicals such as 4-nitrobenzoic acid, thiosemicarbazide, POCl<sub>3</sub>, acetone, ethanol, potassium hydroxide, sodium hydroxide and oxalic acid were procured from Sigma-Aldrich.

## 2.2 Synthesis of 2-amino-5-(4-nitrophenyl)-1,3,4-thiadiazole (ANPT)

A mixture of 4-nitrobenzoic acid (0.01 mol), thiosemicarbazide (0.01 mol) and POCl<sub>3</sub> (10 mL) was refluxed at 85 °C for 2 hrs. The reaction mixture was then cooled to room temperature and 50 mL ice cold water was added. Again, the mixture was refluxed for 4 hrs. After cooling, the mixture was then alkalized to pH 8 by the dropwise addition of 10 % KOH solution. The crude solid precipitate was filtered, washed and dried over a desiccator and purified by recrystallization from ethanol. A yellow compound was obtained with a 75 % yield. The compound's melting point was recorded as 248-252 °C [1-2]. The overall reaction is given in **Figure 2. 1**.

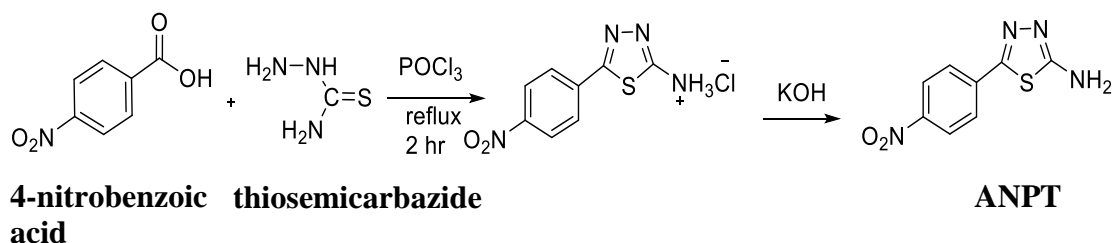


**Figure 2. 1** Synthesis route of 2-amino-5-(4-nitrophenyl)-1,3,4-thiadiazole (ANPT)

## 2.3 Method of Solution Preparation

The stock solution of different chemicals with desired concentration was prepared. Using the stock solutions, other solutions with desired concentrations were prepared by using the dilution method. The following equation was used.

$$V_1S_1 = V_2S_2$$

It was ensured that the distilled water, used for various dilute solutions preparation, was contaminant free.

### 2.3.1 Preparation of Stock Solution of HCl

A stock solution of HCl was prepared by taking the required amount of HCl in a 250 mL volumetric flask, and DI water was added up to the mark to make it a 250 mL solution. Thus 0.5 M concentration of HCl was prepared and used for the electrochemical study. Before every electrochemical or weight-loss test, the concentration of HCl was ensured through acid-base titration, where 0.5M standard NaOH was used as a base.

### 2.3.2 Preparation of CTAB solution

A solution of CTAB was prepared by dissolving the required quantity in 0.5 M HCl in a 250 mL volumetric flask. This CTAB solution was used as a solvent in ANPT solution preparation.

### 2.3.3 Preparation of ANPT solution

ANPT solutions were prepared in a 25 mL volumetric flask using 0.5 M HCl solution as solvent. The required quantity of the ANPT was weight in a balance to prepare solutions with several concentrations; blank, 100 ppm, 200 ppm and 300 ppm. Furthermore, mixture solutions of ANPT with the mentioned concentrations were prepared in 1 mM CTAB solution.

## 2.4 Instruments

The following instruments were used for this study:

1. Digital Balance (AB 265/S/SACT METTLER, Toletto, Switzerland)
2. Shaker machine (Stuart, Orbital shaker, SSL1, United Kingdom)
3. Hot plate & magnetic stirrer (Sniders, 34532, India)
4. Field Emission Scanning Electron Microscopy (FM-SEM) (JEOL JSM-7600F, Tokyo, Japan)
5. Electrochemical Workstation (CHI-660E instruments, USA)

## 2.5 Cells and Electrodes

The electrochemical study was conducted using a three-electrode system ( **Figure 2. 2**) electrochemical cell with the following electrodes:

1. Carbon Steel Rod (WE) (Fe 93.40 %, C 0.24 %, Ni 2.00%, Si 1.57 %, Mn 1.77 %, Cu 0.15 %, Cr 0.33 %, Mo 0.4 %)
2. Platinum Electrode (PtE) (CHI-660E instruments, USA)
3. Silver/Silver Chloride Electrode (Ag/AgCl RE) (CHI-660E instruments, USA)



**Figure 2. 2** Three-electrode system

## 2.6 Preparation of Working Electrode

Rod like CS has been used as the WE (**Figure 2. 3**) in this research. The CS used in the electrochemical studies had 0.28 cm<sup>2</sup> of exposed surface area; the remainder was embedded in Teflon and shrinkable tubes. The surface of the CS specimens was repeatedly abraded with abrasive paper from 120 up to 360 grit size, washed with DI water, degreased with anhydrous ethanol, and then dried at room temperature before each measurement [3, 5].



**Figure 2. 3** Working electrode (CS)

## **2.7 Test Method**

All electrochemical tests were carried out using CHI 660E in a standard three-electrode cell. The weight-loss measurement was performed in an orbital shaker. After completing a weight-loss test, the metal surface was forwarded for FM-SEM analysis.

### **2.7.1 WL Measurement**

The WL technique is one of the physical techniques of corrosion measurement. After performing all the electrochemical tests, the weight-loss test was performed. In this test, CS coins with a diameter of 0.61 cm were immersed in 25 mL of the testing solutions with or without ANPT over 3 hours. At different temperatures and concentrations of ANPT, the test was performed.

### **2.7.2 Surface Analysis**

After weight-loss tests, the CS coins were cleaned with DI water and dried by blowing with cool air for further surface analysis. The surface morphologies and chemical compositions of fresh and corroded samples were examined using FE-SEM and EDX.

### **2.7.3 Electrochemical Analysis**

Electrochemical tests such as OCP, PDP and EIS were performed in this work.

#### **2.7.3.1 OCP**

OCP measurement was performed to obtain a primary idea of the interaction of ANPT and CS in the presence and absence of CTAB. Any external force was not applied during this technique. Only the voltage measurement was available on the cell, but it was disconnected from the power amplifier. The stable potential was recorded and a graph of time versus voltage of the cell was plotted where time was on the X-axis and voltage of the cell was on Y-axis. It was observed that the electrochemical cell reached a steady state almost after 25-30 min.

#### **2.7.3.2 PDP**

PDP was performed after OCP measurements. Before each test, the CS was immersed in the testing solutions for 30 min in the presence and absence of ANPT. The potential

was scanned from a positive to a negative direction. A potential was applied within the range of -150mV to 150mV versus the OCP with a scan rate of  $0.5\text{mV s}^{-1}$  [4].

### **2.7.3.3 EIS Measurement**

EIS tests were performed after OCP and PDP tests. This test provides information about resistance change on the CS surface by applying a range of frequencies. All the EIS tests were performed with a 10 mV amplitude signal from 100 kHz to 100 mHz. there are two parts in the EIS test, (a) Nyquist plot and (b) Bode plot [4].

The Nyquist plot provides information about resistances such as  $R_s$ ,  $R_{ct}$  and different kinds of capacitance such as  $C_{dl}$ . The Nyquist plots were recorded and fitted with a simplified equivalent circuit to acquire more accurate findings about resistance between the ANPT and CS interface [5]. Compared to the Nyquist plot, where frequency values are implicit rather than explicit, the Bode plot gives a clearer representation of the frequency-dependent behavior of the electrochemical system.

## Reference

- [01] CT Keerthi Kumar, J. Keshavayya, T.N. Rajesh, S.K. Peethambar and A.R. Shoukat Ali, "Synthesis, characterization, and biological activity of 5-phenyl-1, 3, 4-thiadiazole-2-amine incorporated azo dye derivatives," *Org. Chem. Int.*, vol. 2013, pp. 1-7, 2013.
- [02] M. Amir, A. Kumar, I. Ali and S.A. Khan, "Synthesis of pharmaceutically important 1, 3, 4-thiadiazole and imidazolinone derivatives as antimicrobials," *Indian J. Chem.*, vol. 48B, pp. 1288-1293, 2009.
- [03] H. Ouici, M. Tourabi, O. Benali, C. Selles, C.nJama, A. Zarrouk and F. Bentiss, "Adsorption and corrosion inhibition properties of 5-amino 1,3,4-thiadiazole-2-thiol on the mild steel in hydrochloric acid medium: Thermodynamic, surface and electrochemical studies," *J. Electroanal. Chem.*, vol. 803, pp. 125–134, 2017.
- [04] S. Varvara, L. M. Muresan, K. Rahmouni, and H. Takenouti, "Evaluation of some non-toxic thiadiazole derivatives as bronze corrosion inhibitors in aqueous solution," *Corros. Sci.*, vol. 50, pp. 2596–2604, 2008.
- [05] S. Xue and Z. Xue, "Microwave-assisted one-pot synthesis and performance test of novel thiadiazole derivatives as an inhibitor of oil transportation pipelines," *Anti-Corros. Methods Mater.*, vol. 64, pp. 461–464, 2017.

### **3. CHAPTER RESULTS & DISCUSSION**



### 3.1 Synthesis of 2-amino-5-(4-nitrophenyl)-1,3,4-thiadiazole (ANPT)

A mixture of 4-nitrobenzoic acid & thiosemicarbazide was refluxed at 85 °C for 2 hrs in presence of solvent POCl<sub>3</sub>. 4-nitrobenzoic acid contains the nitro-phenyl group and the thiosemicarbazide provides the C-S-C bond in ANPT. The solvent POCl<sub>3</sub> was used for cyclilization of the thiadiazole ring. The reaction mixture was then cooled to room temperature and 50 mL ice cold water was added. Again, the mixture was refluxed for 4 hrs. The mixture then forms a water-soluble amonium chloride salt. The mixture was then alkalized to pH 8 by the addition of 10 % KOH solution. In the basic media the synthesized compound, ANPT was precipitated. The crude solid precipitate was filtered, washed and dried over a desiccator and purified by recrystallization from ethanol [1-2]. The overall reaction is given in **Figure 3. 1**.

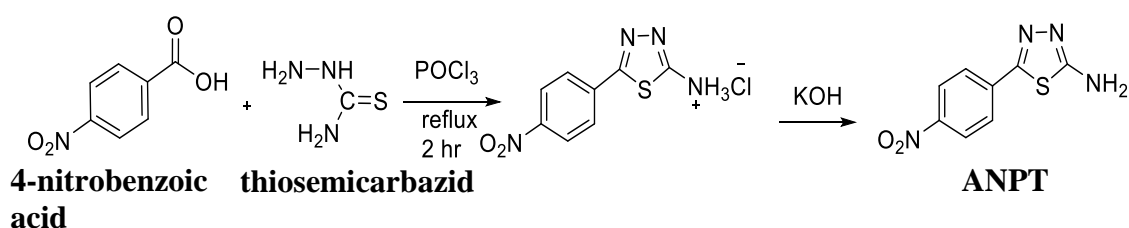


**Figure 3. 1** Synthesis route of 2-amino-5-(4-nitrophenyl)-1,3,4-thiadiazole (ANPT)

The obtained structure was then confirmed by FT-IR and NMR. The IR spectrum (**Figure 3. 2**) of ANPT showed an absorption band at 3289, 3109 cm<sup>-1</sup> for secondary N-H moiety. The aromatic C-H stretching was detected at 2792, 2709 cm<sup>-1</sup>. The peak at 1635 cm<sup>-1</sup> indicates C=N stretching. The characteristic peak at 1507 cm<sup>-1</sup> was distinguished and observed for aromatic C=C and the peak at 619 cm<sup>-1</sup> was for C-S-C stretching.

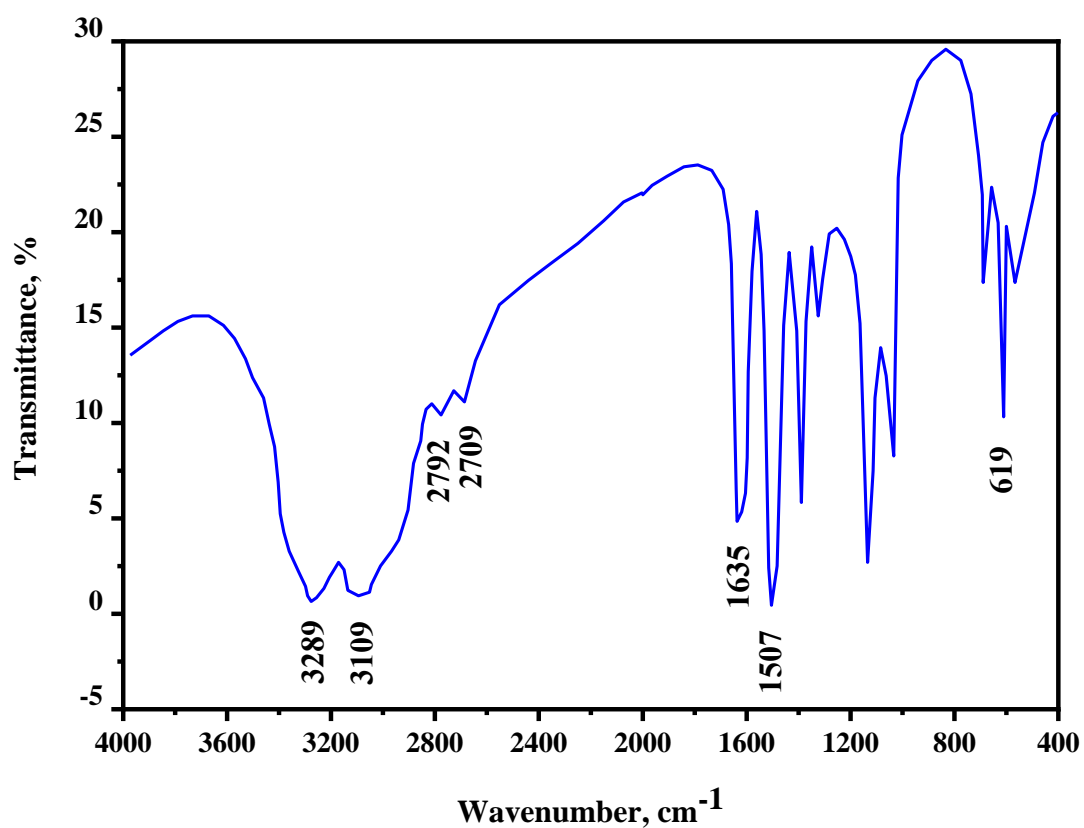


**Figure 3. 2** FT- IR spectrum of ANPT

The <sup>1</sup>H NMR spectra (**Figure 3. 3**) of ANPT showed a sharp singlet for the N-H proton at  $\delta$  7.559. The doublet with coupling constant  $J=8.0$  Hz was designated at  $\delta$  8.05, 8.07 was attributed for two aromatic protons, and another doublet with coupling constant  $J=8.0$  Hz was assigned at  $\delta$  8.17,8.19 for two aromatic protons. A sharp singlet attributed at 7.284 is for CDCl<sub>3</sub> which is used as the solvent. However, the presence of six protons was confirmed in ANPT by <sup>1</sup>H NMR analysis.

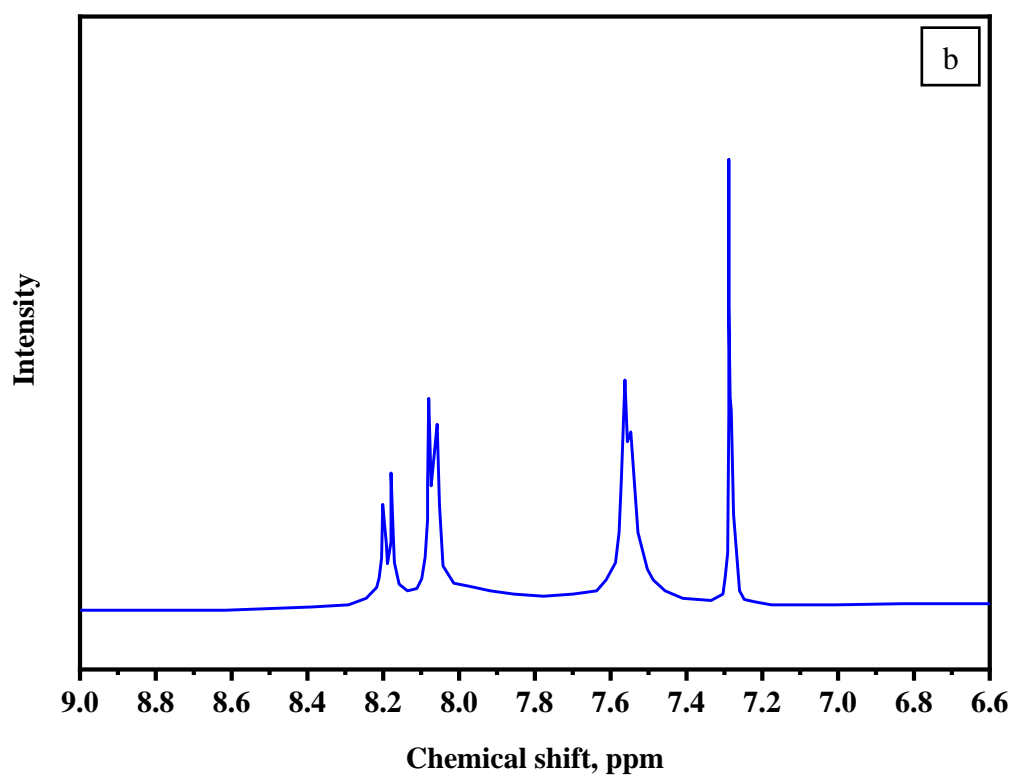
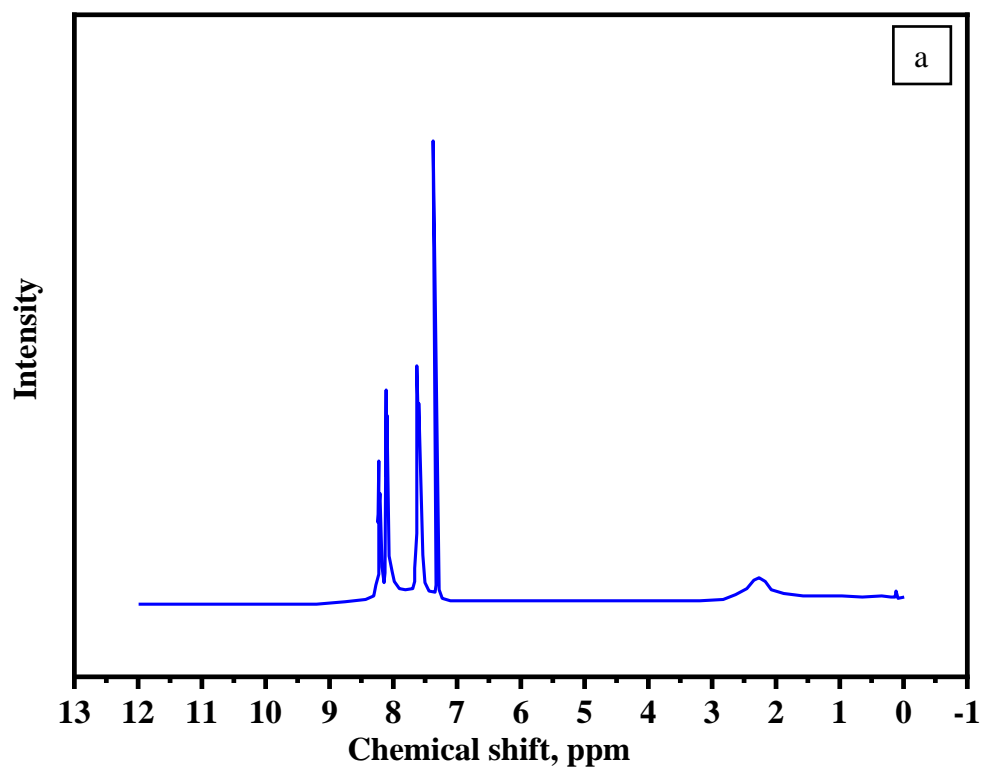


**Figure 3. 3** NMR Spectra of ANPT (a) NMR spectra (b) expanded NMR spectra

### 3.2 Weight-Loss Test

The  $CR$  of CS and the percentage of  $IE$  were calculated by the WL test with different concentrations (100-250 ppm) of ANPT for 3 hours [3-5]. This test was performed at room temperature (298 K) and data is presented in **Table 3. 1**. The values of  $CR$ ,  $IE$  and  $\theta$  was calculated by using the equations 1, 2 and 3.

**Table 3. 1** Corrosion parameters for CS immersed in 0.5M HCl solution for 3h without/with different concentrations of ANPT at 298 K temperature obtained from WL measurements

$C_{inh}$ (ppm)	$\Delta W$ (mg)	$CR$ ( $mgcm^{-2}h^{-1}$ )	$IE_{WL}$ (%)	$\theta$
Blank	65	37	---	---
100	31	18	52	0.52
150	22	13	67	0.67
200	17	10	74	0.74
250	12	7	81	0.81

This table shows that the  $CR$  decreased with the increase in the concentration of ANPT. In the HCl solution, the  $CR$  of the CS was  $37 mgcm^{-2}h^{-1}$  in absence of ANPT. Then with the addition of only 100 ppm ANPT  $CR$  was dropped to  $18 mgcm^{-2}h^{-1}$ , half of the initial  $CR$ . But, after that no significant change in  $CR$  was observed by the presence of 150 ppm, 200 ppm and 250 ppm ANPT. However, at a concentration of 100 ppm of ANPT, the  $IE$  % was 52 %, which increased with the addition of CI. The  $IE$  % increased to 81 % at a concentration of 250 ppm. The increased surface coverage by the ANPT molecules at the CS/acid solution interface through adsorption is thought to be responsible for corrosion inhibition [4, 6-7]. The  $CR$  of CS decreases with the increasing surface coverage by ANPT in 0.5M HCl solution after 3 hours of immersion. After WL analysis the surface morphology of the CS coins were observed by FE-SEM analysis technique.

### 3.3 FE-SEM Analysis of CS Surfaces:

FE-SEM was used to analyze the adsorption layer's CS surface morphology both in the absence and presence of ANPT in 0.5 M HCl solution [8, 9]. **Figure 3. 4** shows the FE-SEM images at 10  $\mu m$  magnification of the normal CS surface, corroded CS surface

dipped in 0.5 M HCl solution and CS surface dipped in 0.5 M HCl solution in presence of 200 ppm ANPT. From the figure, it is seen that, before immersion of CS in ANPT solution, it was a clean and smooth surface, which became damaged because of corrosion, and rust surfaces were observed in various points for the immersion in 0.5 M HCl solution. While it showed a less corroded surface in presence of the 200 ppm ANPT solution. These results demonstrated that inhibitors formed a surface-adsorbed layer that shields the CS from acid attack and inhibits the material's damage, thereby reducing corrosion. To analyze the adsorption nature, adsorption isotherm was observed.

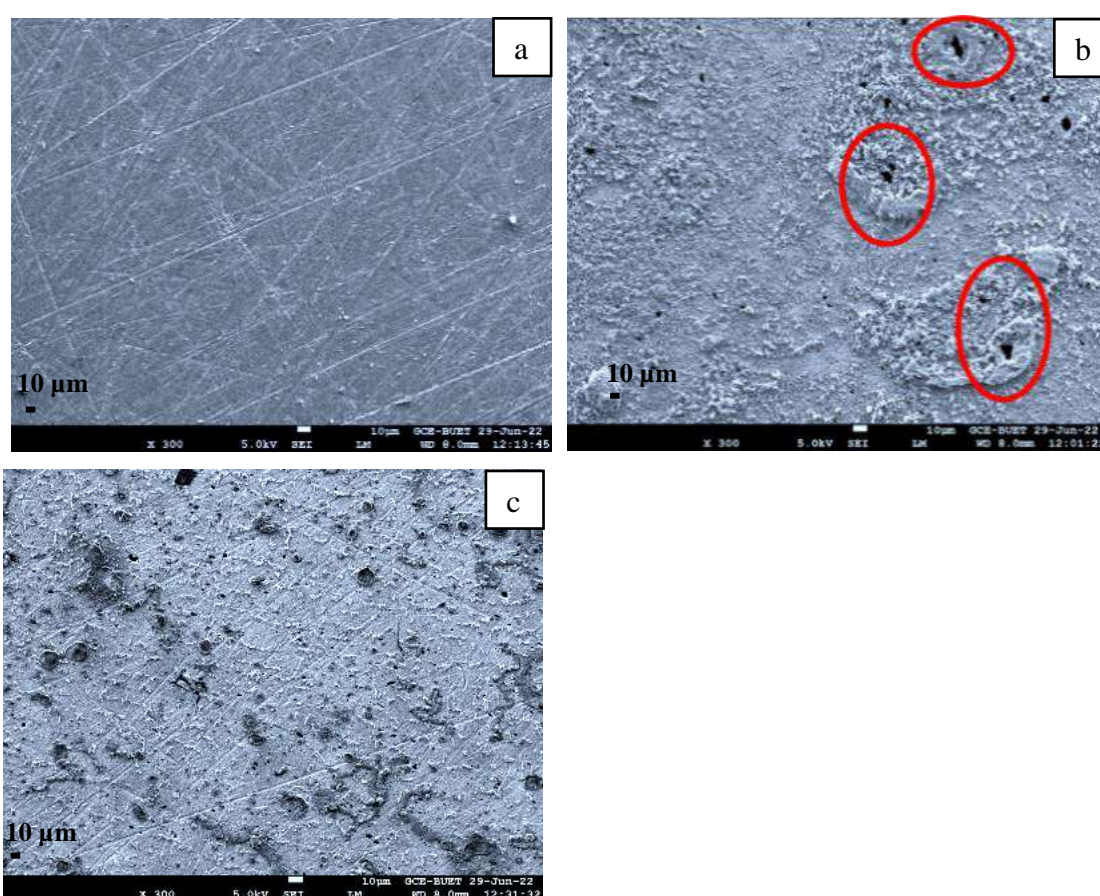


**Figure 3. 4** SEM images of CS surface (a) before immersion (b) corroded surface after immersion 0.5 M HCl solution (c) in presence of 200 ppm ANPT

### 3.4 Adsorption Isotherm

Adsorption isotherms are also analyzed by WL. According to the Langmuir adsorption isotherm,  $\theta$  is related to the inhibitor concentration and adsorption equilibrium constant. Rewriting equation 4, the following equation is observed [6],

$$\frac{C_{inh}}{\theta} = \frac{1}{K_{ads}} + C_{inh}$$

where  $K_{ads}$  is the adsorptive equilibrium constant and  $C_{inh}$  is the concentration of inhibitor [10-13]. The values of  $C_{inh}$  and  $\theta$  at different temperatures are presented in **Table 3. 2**.

**Table 3. 2** The values of  $C_{inh}$  and  $\theta$  at different temperatures

$C_{inh}$ (ppm)	Temperature (K)							
	298		303		313		323	
	$\theta$	$C_{inh}/\theta$	$\theta$	$C_{inh}/\theta$	$\theta$	$C_{inh}/\theta$	$\theta$	$C_{inh}/\theta$
100	0.52	192.27	0.92	108.44	0.89	112.05	0.81	122.14
150	0.67	227.85	0.93	161.2	0.88	168.84	0.78	191.84
200	0.74	269.32	0.96	206.86	0.88	225.45	0.72	274.83
250	0.81	306.74	0.94	265.33	0.90	277.42	0.81	306.15

A plot of experimental data expressed as  $C_{inh}/\theta$  vs.  $C_{inh}$  yielded straight lines presented in **Fig. 3. 5**. The linear correlation coefficient ( $R^2$ ) is greater than 0.9 (**Table 3. 3**). The adsorptive equilibrium constant ( $K_{ads}$ ) had been be calculated from the reciprocal of the intercept of the  $C_{inh}/\theta$  vs  $C_{inh}$  curve [4].

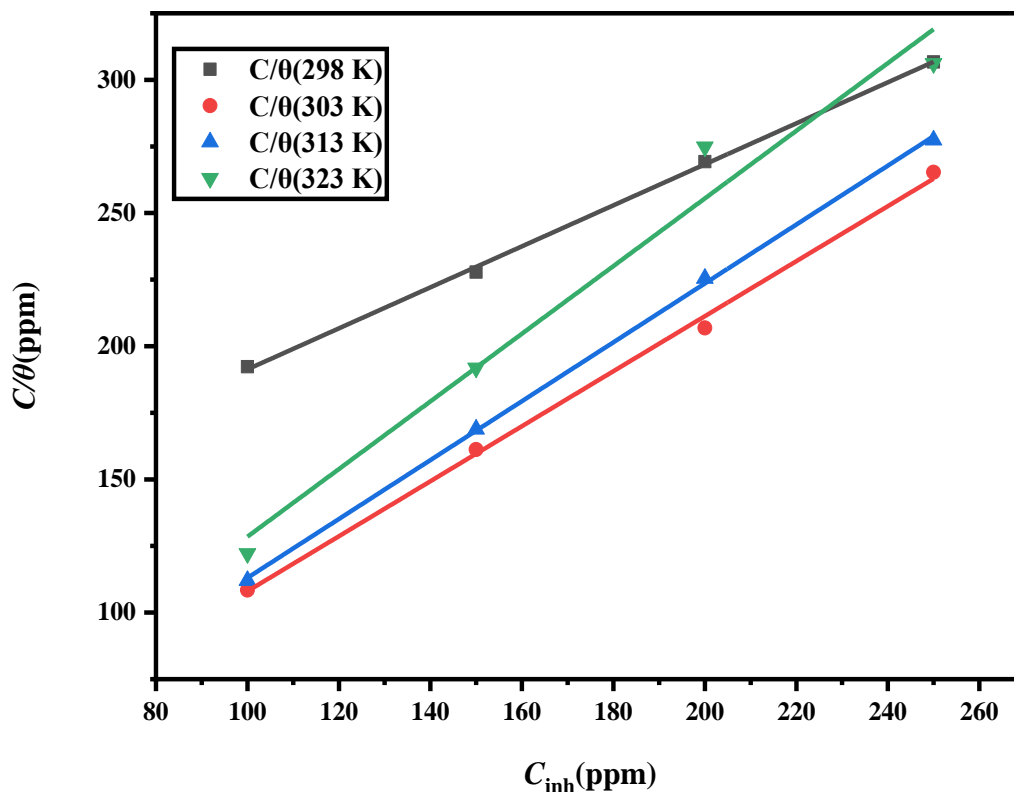


**Figure 3. 5** Langmuir adsorption model of various concentrations of ANPT on the surface of CS in 0.5 M HCl at different temperatures

In Langmuir adsorption isotherm, Gibb's free energies had been calculated from the intercept of the curves. It can be observed that the value of  $\Delta G_{ads}^0$  calculated from these data is negative, indicating the spontaneous adsorption of ANPT molecules on the CS surface. Moreover, Gibb's free energies at temperatures 303 K, 313 K and 323 K are below  $-20 \text{ kJmol}^{-1}$ , which indicates the physisorption. Because, if the free energy of activation is less than  $-20 \text{ kJmol}^{-1}$ , then the adsorption nature is supposed to be physical, which is due to the electrostatic interaction between the charged molecules and charged metal surface [14]. In contrast, around  $-40 \text{ kJmol}^{-1}$  or a higher value of Gibb's free energy indicates chemisorption involving charge sharing or transfer from organic molecules to the metal surface to form a coordinate type of bond [14-16].

**Table 3. 3** Adsorption parameters of ANPT and CS surface in 0.5 M HCl by Langmuir adsorption isotherm at different temperatures (298 K, 303 K, 313 K, 323 K)

Temperature (K)	Intercept	Slope	$R^2$	$K_{ads}$	Free energy of adsorption, $\Delta G_{ads}^0$ (kJmol <sup>-1</sup> )
298 K	114.33	0.76	0.99	0.00	1.80 kJmol <sup>-1</sup>
303 K	4.74	1.03	0.99	0.21	-6.19 kJmol <sup>-1</sup>
313 K	2.48	1.10	0.99	0.40	-8.08 kJmol <sup>-1</sup>
323 K	1.48	1.27	0.97	0.67	-9.73 kJmol <sup>-1</sup>

The value of Gibbs free energy at temperatures 303 K, 313 K and 323 K were -6.19 kJmol<sup>-1</sup>, -8.08 kJmol<sup>-1</sup>, and -9.73 kJmol<sup>-1</sup> respectively. It is clear from the above explanation that the adsorption type of ANPT molecule on the CS surface is **physisorption**. To find the best fit, the Temkin adsorption isotherm was checked. In Temkin adsorption isotherm, the adsorption parameter is calculated by rewriting equation 6 [11]:

$$\theta = -\frac{1}{g} \ln C_{inh} - \frac{1}{g} K_{ads}$$

Where  $g$  is the molecular interaction parameter. A plot of experimental data expressed as  $\theta$  vs.  $\ln C_{inh}$  yielded straight lines (**Fig. 3. 6**). The values of  $C_{inh}$ ,  $\ln C_{inh}$  and  $\theta$  at different temperatures are presented in **Table 3. 4**.

**Table 3. 4** The values of  $C_{inh}$ ,  $\ln C_{inh}$  and  $\theta$  at different temperatures

$C_{inh}$ (ppm)	$\ln C_{inh}$ (ppm)	$\theta$			
		298 K	303 K	313 K	323 K
100	4.6	0.52	0.92	0.89	0.81
150	5.01	0.67	0.93	0.88	0.78
200	5.29	0.74	0.96	0.88	0.72
250	5.52	0.81	0.94	0.90	0.81

The linear correlation coefficient ( $R^2$ ) value along with intercept and slope had been tabulated in **Table 3. 5**.



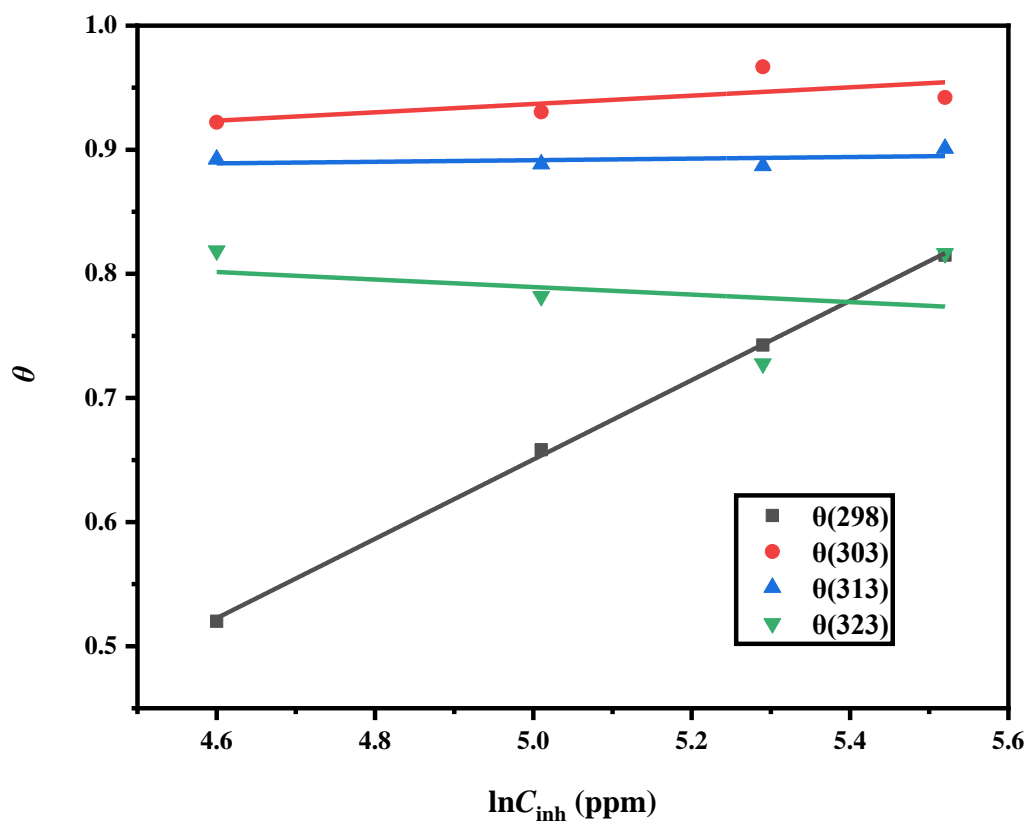


**Figure 3. 6** Temkin isotherm adsorption model of various concentrations of ANPT on the surface of CS in 0.5 M HCl at different temperatures

**Table 3. 5** Adsorption parameters of ANPT and CS surface in 0.5 M HCl by Temkin adsorption isotherm at different temperatures (298 K, 303 K, 313 K, 323 K)

Temperature (K)	Intercept	Slope	$R^2$
298	-0.94	0.3197	0.99
303	0.76	0.0336	0.46
313	0.85	0.0064	0.16
323	0.94	-0.0302	0.07

The linear correlation coefficient ( $R^2$ ) in the conducted data from **Figure 3. 6** is less than 0.9. In this sense, this adsorption is found to be unfit for this system.

From the Freundlich adsorption isotherm, the adsorption parameter was also calculated by the given equation 5 [12]. A plot of experimental data expressed as  $\ln\theta$  vs.  $\ln C_{inh}$  yielded straight lines (**Fig. 3. 7**). The linear correlation coefficient ( $R^2$ ) is equal to 1

(Table 3. 7). The values of  $C_{inh}$ ,  $\ln C_{inh}$  and  $\theta$  at different temperatures are presented in Table 3. 6.

**Table 3. 6** The values of  $C_{inh}$ ,  $\ln C_{inh}$  and  $\theta$  at different temperatures

$C_{inh}$ (ppm)	$\ln C_{inh}$ (ppm)	Temperature (K)							
		298		303		313		323	
		$\theta$	$\ln \theta$	$\theta$	$\ln \theta$	$\theta$	$\ln \theta$	$\theta$	$\ln \theta$
100	4.6	0.52	-0.65	0.92	-0.08	0.89	-0.11	0.81	-0.2
150	5.01	0.67	-0.41	0.93	-0.07	0.88	-0.11	0.78	-0.24
200	5.29	0.74	-0.29	0.96	-0.03	0.88	-0.11	0.72	-0.31
250	5.52	0.81	-0.20	0.94	-0.05	0.90	-0.10	0.81	-0.20

The adsorptive equilibrium constant ( $K_{ads}$ ) can be calculated from the intercept of the  $\log \theta$  vs.  $\log C_{inh}$  curve. The value of  $\frac{1}{n}$  indicates the ease of adsorption. Generally, if the value is between  $0 < \frac{1}{n} < 1$ , then the adsorption is thought to be easy and moderate. If the value of  $\frac{1}{n}$  is greater than 1 then the adsorption process is supposed to be difficult [12].

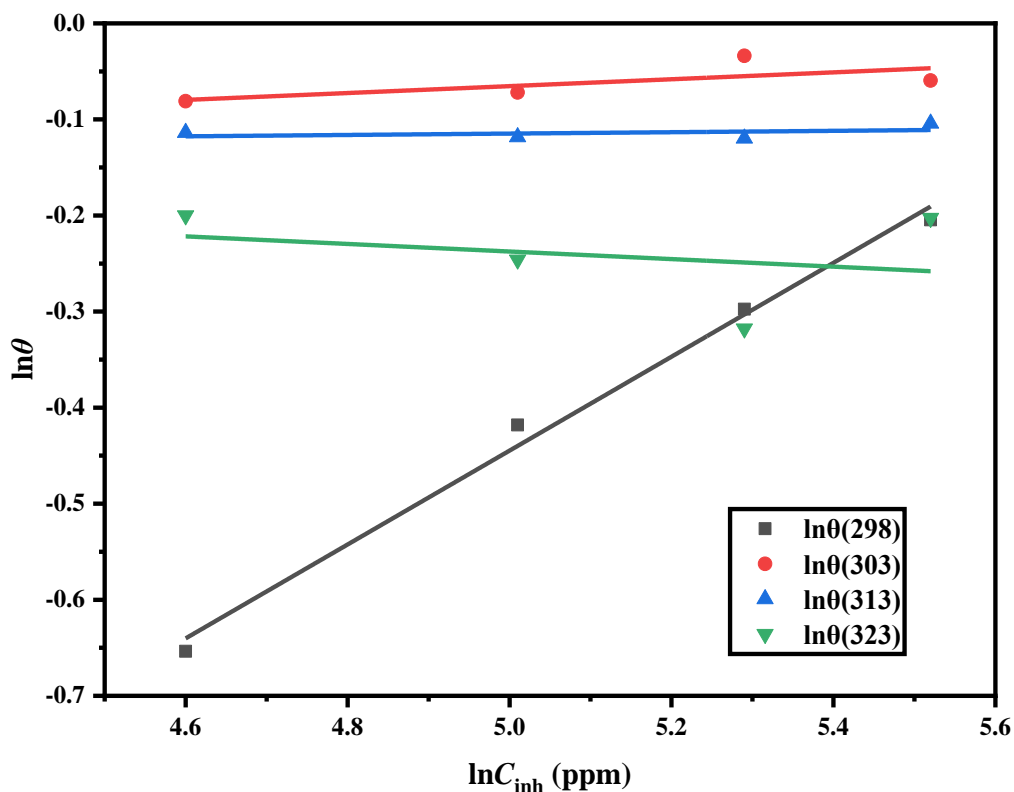


**Figure 3. 7** Freundlich isotherm adsorption model of various concentrations of ANPT on the surface of CS in 0.5 M HCl at different temperatures

**Table 3. 7** Adsorption parameters of ANPT and CS surface in 0.5M HCl by Freundlich adsorption isotherm at different temperatures (298K, 303K, 313K, 323K)

$\ln \theta$ (ppm)	Intercept	Slope	$R^2$
298 K	-2.88	0.4886	0.99
303 K	-0.24	0.0358	0.47
313 K	-0.15	0.0071	0.16
323 K	-0.04	-0.0394	0.08

In this table it is observed that the linear correlation coefficient ( $R^2$ ) is less than 0.9 indicating this adsorption is found to be unfit for this system.

From the above discussion, it's clear that the adsorption nature between ANPT and CS surface in 0.5 M HCl is followed by Langmuir adsorption isotherm and the adsorption type is **physisorption**. To understand the adsorption nature more elaborately, the activation energy, enthalpy and entropy value were calculated by thermodynamic characterizations.

### 3.5 Thermodynamic Characterization

Temperature is an important parameter in studies of corrosion inhibition [17]. The effect of temperature on adsorption was studied in 0.5 M HCl at the temperature range of 298 K to 323 K in the absence and presence of ANPT for 3 hours. The data was calculated by the WL experiment and presented in **Table 3. 8**.

**Table 3. 8** Corrosion parameters for CS immersed in 0.5 M HCl solution for 3 hours without/with ANPT at 298 K, 303 K, 313 K & 323 K temperature obtained from WL measurements

$C_{inh}$ (ppm)	Temperature (K)							
	298		303		313		323	
	CR	IE <sub>WL</sub>	CR	IE <sub>WL</sub>	CR	IE <sub>WL</sub>	CR	IE <sub>WL</sub>
<b>Blank</b>	0.0373	---	0.0475	---	0.0753	---	0.1032	---
<b>100</b>	0.0179	52	0.0037	92	0.0081	89	0.0187	81
<b>150</b>	0.0127	67	0.0033	93	0.0084	88	0.0225	78
<b>200</b>	0.0096	74	0.0015	96	0.0085	88	0.0281	72
<b>250</b>	0.0069	81	0.0027	94	0.0074	90	0.0189	81

When the temperature increases from 298 K to 303 K, the IE keeps rising, whereas, after that, IE was dropped down. The increase in IE with increasing temperature is observed between temperatures 298K to 303K and after that, a decrease in IE is found there. This revealed that desorption occurs at the CS surface at high temperatures. After 303 K, the CR increases with the rise of temperature. At 303K temperature, the highest IE value is observed for 200 ppm ANPT. In this case, the electrostatic interaction between the inhibitor molecules and the CS surface generates an attraction between them through physisorption. The activation parameters for the corrosion reactions were calculated from the Arrhenius-type plot by using equation 9 [4].

The values of  $E_a$  for CS in 0.5 M HCl with and without ANPT obtained from the slope of the plots  $\ln(CR)$  vs.  $1000/T$  have shown in **Figure 3. 8**. The data obtained from this figure, are listed in **Table 3. 9**. The energy of activation,  $E_a$  was calculated by using the data obtained from that figure. The change in  $E_a$  value contains important information about the nature of the adsorption of inhibitor molecules on the metal surface.

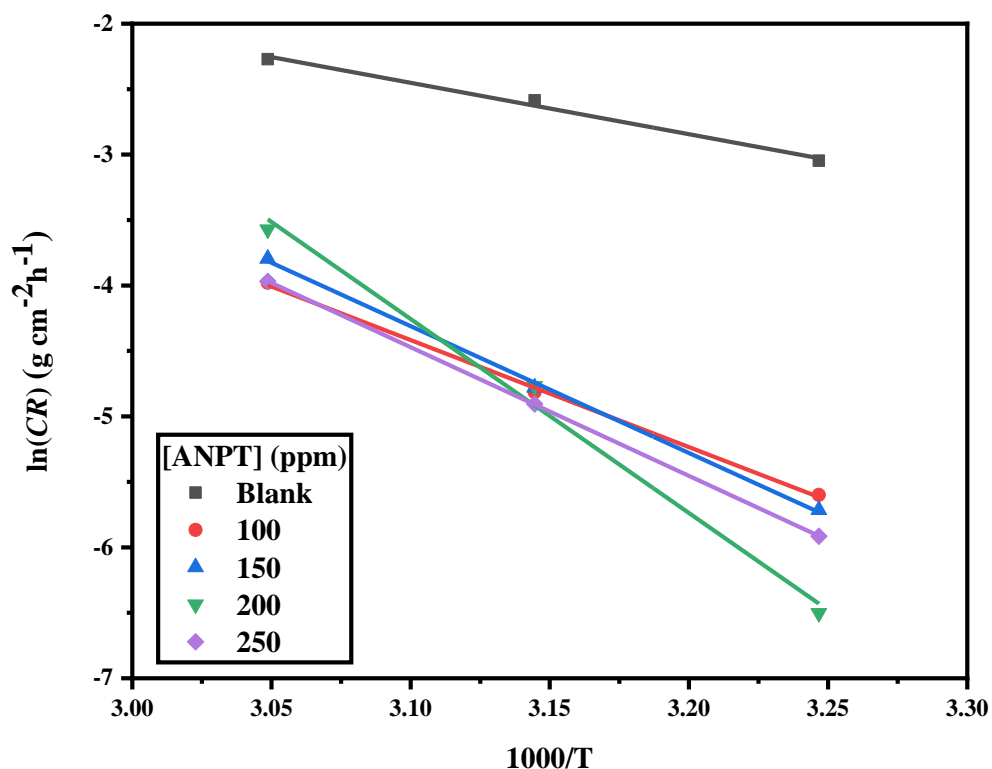


**Figure 3. 8** Arrhenius Plot for CS in 0.5 M HCl solution without and with ANPT at different concentrations of ANPT

**Table 3. 9** The activation energy of adsorption on the CS surface in the absence and presence of ANPT at different concentrations was calculated by Arrhenius Plot

$C_{inh}$ (ppm)	Slope	$E_a$ (kJmol <sup>-1</sup> )
Blank	- 3.92	33
100	-8.17	68
150	-9.68	81
200	-14.82	123
250	-9.82	82

In this table, it is observed that the  $E_a$  value for the inhibited system by 200 ppm ANPT was four times greater than the uninhibited system.

Generally increased  $E_a$  indicates physical adsorption which occurs in the first stage by weak chemical bonding between the inhibitors and the metal surface [6]. So, the increased  $E_a$  in the presence of 200 ppm ANPT suggested that ANPT reduced the dissolution of CS in 0.5 M HCl through the physical adsorption layer.

Alternative Arrhenius plots of  $\ln(CR/T)$  vs  $1000/T$  (**Figure 3. 9**) for CS dissolution in 0.5 M HCl both in absence and presence of ANPT at different concentrations were used to calculate the value of activation enthalpy ( $\Delta H_a^\circ$ ) using equation 11 [19]. Straight lines were also obtained from this plot with a linear correlation coefficient ( $R^2$ ) value which was around 1.

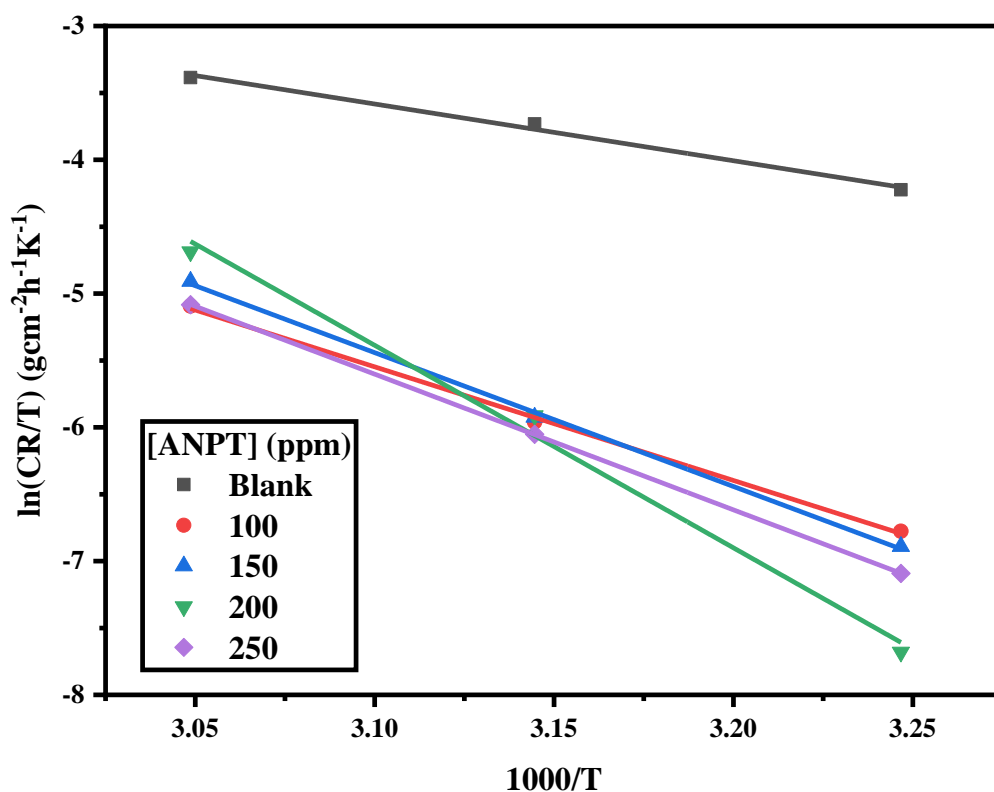


**Figure 3. 9** Alternative Arrhenius Plot of  $\ln(CR/T)$  vs.  $1000/T$  for CS in 0.5 M HCl solution without and with different concentrations of ANPT

The value of  $\Delta H_a^\circ$  was calculated from the slope of the  $\ln(CR/T)$  vs.  $1000/T$  plot and intercept was used to calculate the value of  $\Delta S_a^\circ$ . The calculated value of  $\Delta H_a^\circ$  and  $\Delta S_a^\circ$  obtained from these plots are tabulated in **Table 3. 10**.

**Table 3. 10** Some thermodynamic parameters for the adsorption of ANPT on the CS surface

$C_{inh}$ (ppm)	$E_a$ (kJmol <sup>-1</sup> )	$\Delta H_a^0$ (kJmol <sup>-1</sup> )	$\Delta S_a^0$ (kJmol <sup>-1</sup> )
Blank	33	35	-118
100	68	71	-25
150	81	83	15
200	123	126	148
250	82	84	17

This table shows the value of activation energy of the uninhibited system is lower than the inhibited system of 200 ppm ANPT and CS in 0.5 M HCl solution indicating the physical adsorption between ANPT molecules and CS surface.

The nature of adsorption is assumed by the value of enthalpy  $\Delta H_a^0$ , either it would be endothermic or exothermic. The positive values of  $\Delta H_a^0$  of the system indicate endothermic adsorption [20-21]. In comparison to the values obtained for the uninhibited solution, the presence of the inhibitor results in greater values for  $\Delta H_a^0$ . This suggests improved protection effectiveness. This might be explained by the reaction having an energy barrier, whereby the adsorption process increases the enthalpy of the corrosion process. The value of  $\Delta H_a^0$  at a concentration 200 ppm ANPT is much higher than the uninhibited system revealing a barrier between the ANPT molecule and the CS surface.

Since the activated complex in the rate-determining step represents an association rather than a dissociation step, large and negative values of entropies  $\Delta S_a^0$  imply that this step represents an association rather than a dissociation step, and this implies that there is a reduction in disordering as one moves from reactants to the activated complex [19-22]. In **Table 3. 10**, the  $\Delta S_a^0$  value of the uninhibited system is much more negative than the inhibited one. However, by the addition of 200 ppm ANPT, the value shifted to a more positive side resulting decreasing the *CR*.

The above discussion provides thermodynamic evidence that ANPT effectively prevents CS corrosion in the presence of a 0.5 M HCl solution through adsorption on the CS surface.

By the previous discussion it's observed that in WL analysis at concentration 250 ppm ANPT the highest IE was found. But thermodynamic analysis supports 200 ppm for the highest IE of ANPT in 0.5 M HCl solution. This difference may be due to the abrupt measurement in WL. Furthermore, Electrochemical tests were also performed to observed the IE of ANPT.

### 3.6 Electrochemical Studies

Electrochemical tests such as OCP, PDP Measurement and EIS were performed. All these tests were conducted in a three-electrode system. The test results of these electrochemical techniques are discussed below:

### 3.7 OCP Analysis

Every corrosion reaction has a potential value (OCP) in absence of any supplied current [23]. In this manner, the corrosion reactions of CS in 0.5 M HCl have also an OCP value depending on the nature of the metal and corrosive environment. Then, a change in OCP will happen with the addition of the inhibitor, ANPT.

The open circuit potential (OCP) of CS was measured in 0.5 M HCl solution without and with the addition of different concentration of ANPT at room temperature. The obtained results are shown in **Figure 3. 10**. which represents the variation in open circuit potential with time in the absence and presence of ANPT.



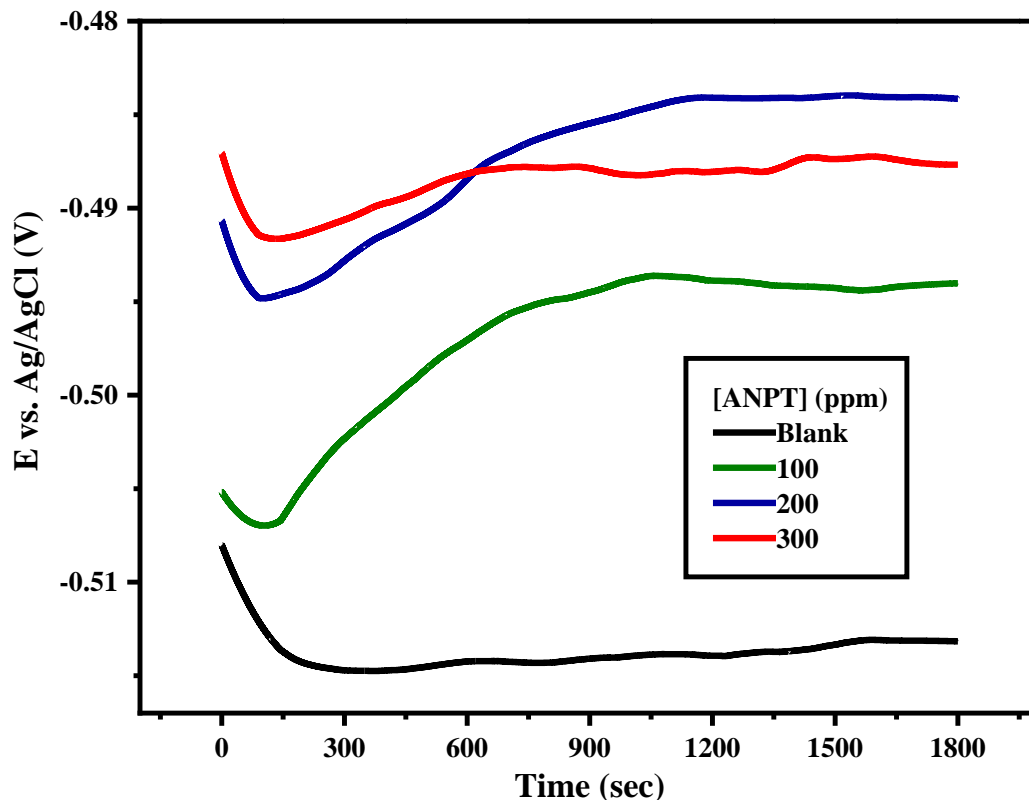


**Figure 3. 10** Time variation of the OCP for CS in 0.5 M HCl solution with different concentrations of ANPT at room temperature

Initially, the OCP value of the CS electrode in inhibitor-free 0.5 M HCl solution seems to be negative shown in curve for 0.5 M HCl solution in **Figure 3. 10**. This negative value signifies the deposition of corrosion products on the CS surface. Moreover, the electrode's potential shifts toward higher negative values than the initial potential indicating the dissolution of the CS electrode in 0.5 M HCl solution [24-25]. After 300 seconds the change in potential is observed almost steady.

The curves for 100 ppm, 200 ppm and 300 ppm in **Figure 3. 10**, represents the variation in OCP of CS in 0.5 M HCl with time after the addition of ANPT at different concentration. All these curves show a more positive value of OCP than the blank one. Though at first, all the curves moved toward a negative value indicating CS dissolution, after around 150 seconds followed the upper trend indicating a decrease in metal dissolution [25]. Almost after 1100 seconds a steady change is observed in all the curves. So, these results attributed that the ANPT formed a protective film on the CS surface immersed in 0.5 M HCl solution. Moreover, at a concentration of 200 ppm of

ANPT in 0.5M HCl solution, the most positive OCP value of CS is found pointing a better *IE* than the other concentrations.

### 3.8 PDP Analysis

The cathodic and anodic polarization curve of CS in 0.5 M HCl in the absence and presence of various concentrations of ANPT at room temperature is presented in **Figure 3. 11**. The scan rate was 0.5 mVs<sup>-1</sup>.

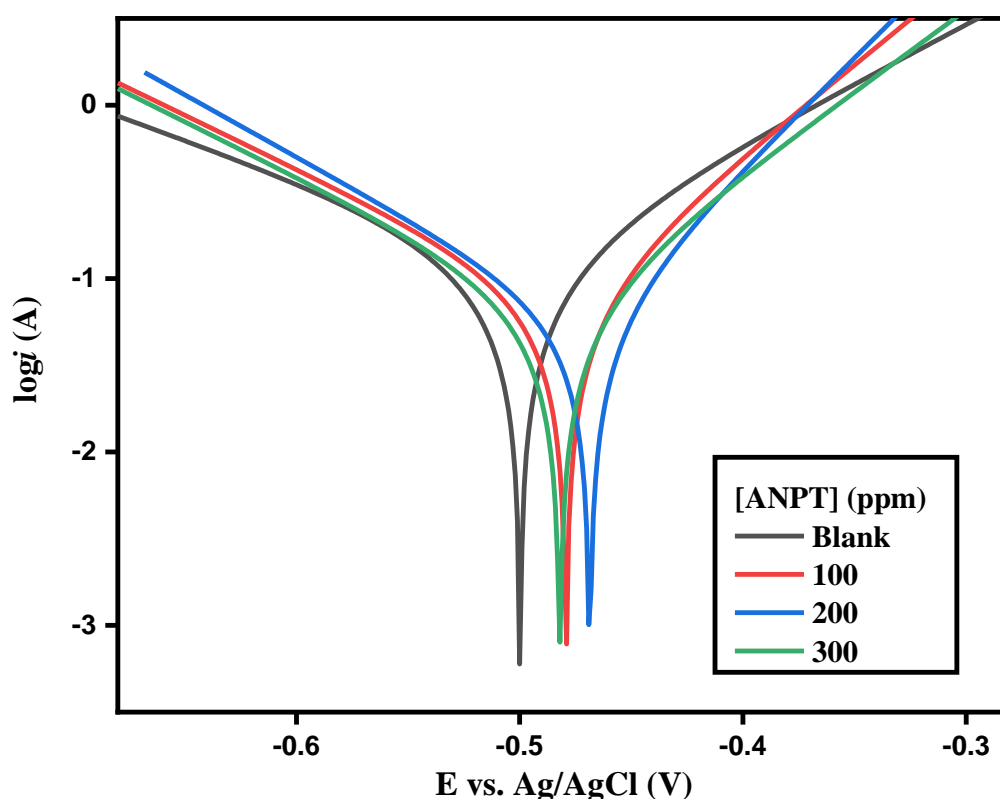


**Figure 3. 11** PDP plots for CS in 0.5 M HCl solution with different concentrations of ANPT at room temperature

Electrochemical kinetic parameters, i.e., corrosion potential ( $E_{\text{corr}}$ ), cathodic and anodic Tafel slope ( $\beta_c$  and  $\beta_a$ ) and corrosion current density ( $i_{\text{corr}}$ ), obtained by extrapolation of the Tafel lines, are presented in **Tale 3. 11**.

**Figure 3. 11** illustrates how the concentration of thiadiazole derivatives affects the cathodic and anodic branches, respectively, and how this influence varies. The  $IE_{\text{PDP}}$  of ANPT for CS against 0.5 M HCl at room temperature has been calculated by using equation 12 [4, 26].

**Table 3. 11** The PDP parameters for CS in 0.5 M HCl solution without/with different concentrations of ANPT at room temperature

$C_{inh}$ (ppm)	$E_{corr}$ (mV)	$i_{corr}$ (mA cm <sup>-1</sup> )	$\beta_c$ (mVdec <sup>-1</sup> )	$\beta_a$ (mVdec <sup>-1</sup> )	IE (%)
Blank	-499.80	1.30	209.6	130.6	---
100	-479.26	0.76	161.0	95.0	42
200	-468.61	0.57	139.4	78.0	56
300	-482.02	0.81	175.4	119.2	38

The table shows the  $E_{corr}$  displacements in the presence and absence of ANPT toward positive value. This indicates the absorption of corrosion inhibitor molecules on the surface of the metal sample leading the formation of a protective layer on the CS surface. Additionally, it demonstrates that the molecules are absorbed across the surface of the mild steel sample more quickly and readily due to the lower density of anodic and cathodic currents [26].

Additionally, the values of the Tafel coefficients ( $\beta_c$ ,  $\beta_a$ ), in the presence of ANPT considerably alter with the inhibitor's concentration, suggesting that these substances have an impact on the kinetics of the anodic and cathodic processes [4].

As can be seen in **Table 3. 11.**, the  $IE$  increased with the increase in the concentration of ANPT in 0.5 M HCl solution. But at the highest concentration, there is a fall in  $IE$ . The best  $IE$  is observed at a concentration of 200 ppm ANPT and the  $IE_{PDP}$  is 56.15 %. Moreover, an inhibitor may only be classified as anodic or cathodic if its  $E_{corr}$  displacement is higher than 85 mV [27]. From **Table 3.11.** the maximum  $E_{corr}$  displacement in presence of 200 ppm ANPT is 31mV, indicating that ANPT is a mixed-type inhibitor. Now it is clear from the above discussion of PDP measurement that ANPT may be utilized as a mixed-type corrosion inhibitor.

### 3.9 EIS Analysis

EIS is a powerful technique having advantages in obtaining some parameters such as the passivation properties of the material, the kinetics of the electron transfer and the representation of the properties of the surface structure and its corrosion phenomena by equivalent circuits [27]. The Nyquist and Bode plots of CS immersed in the acidic

solution in the presence and absence of ANPT at the OCP obtained by EIS are represented in **Figure 3. 12** and **Figure 3. 13**.

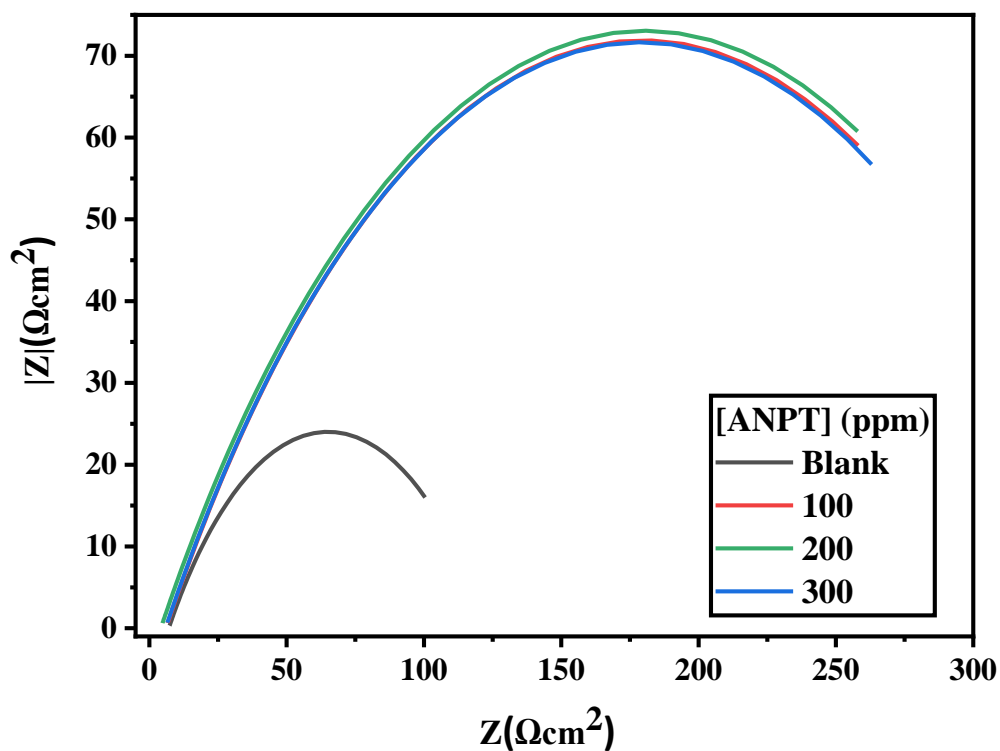


**Figure 3. 12** Nyquist plots for CS in 0.5 M HCl with different concentrations of ANPT

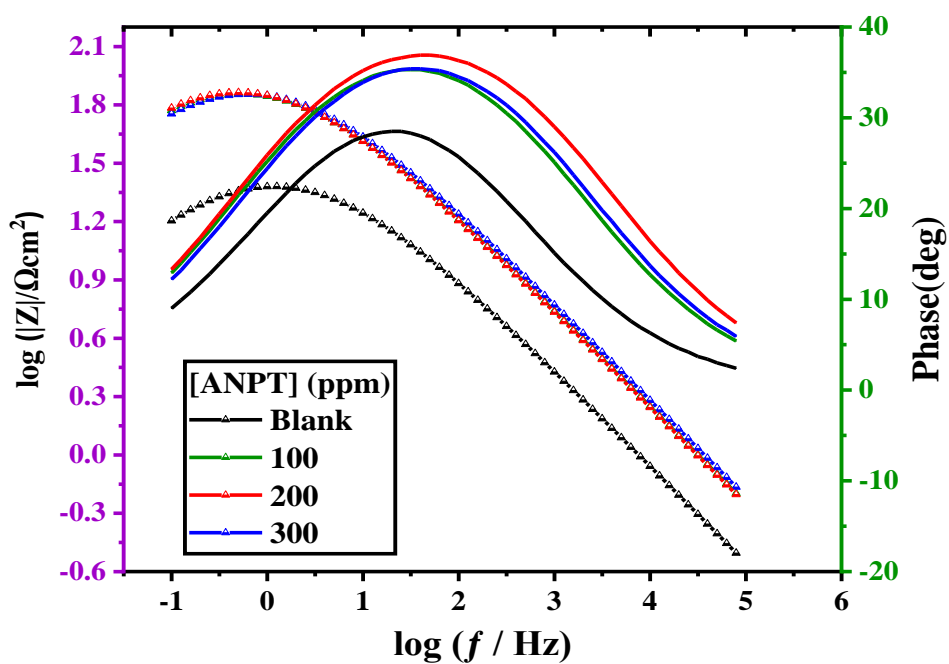


**Figure 3. 13** Bode plots for CS in 0.5 M HCl with different concentrations of ANPT

It can be seen from **Figure 3. 12**, the Nyquist plot shows a depressed semicircle in absence of ANPT and the radius of the semicircle increased with the presence of ANPT within the range of 100 ppm to 300 ppm. Deviation of a perfect semicircle of the Nyquist plot expresses inhomogeneity and roughness of an electrode surface [19] and an increased radius of a Nyquist plot in presence of the inhibitor suggests the *IE* [26]. The random adsorption of ANPT molecules may be responsible for a decrease in steel surface homogeneity arising from the non-uniform film formed on the CS surface. In the presence of ANPT, the semicircles increased indicating the *IE* of ANPT.

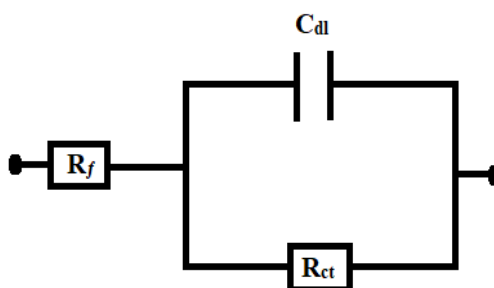


**Figure 3. 14** Equivalent circuit

In **Figure 3. 13**, the Bode plot showed shifting of frequency at maximum phase angle to higher value in the presence of ANPT. The given equivalent circuit in **Figure 3. 14** was used for EIS data fitting [19]. All the impedance data was fitted by the following equivalent circuit. The fitted impedance data are listed in **Table 3. 12**.

**Table 3. 12** Electrochemical impedance parameters for CS in 0.5 M HCl solution with ANPT at different concentrations

$C_{inh}$ (ppm)	$R_f$ ( $\Omega\text{cm}^2$ )	$R_{ct}$ ( $\Omega\text{cm}^2$ )	$IE_{EIS}$ (%)
Blank	7.07	116	---
100	6.06	347	67
200	4.17	353	67
300	5.90	346	66

$R_f$  corresponds to the adsorption of inhibitor on the metal surface and  $R_{ct}$  ascribe electron transfer on the metal solution interface. In impedance plots at high frequencies  $R_f$  and  $R_{ct}$  at low frequencies can be appeared [27].

**Table 3. 12** shows the value of  $R_{ct}$  increased with the increasing concentration of ANPT within the range of 100 ppm to 300 ppm. An increase in  $R_{ct}$  value indicates the increase

of inhibitor molecules' adsorption on the metal surface [19]. The higher  $R_{ct}$  value for ANPT was found at a concentration of 200 ppm and the best  $IE$  ( $IE_{EIS}$  %) is 67.11 %. Hence, these results may be attributed to the adsorption of ANPT forming a protective adsorption layer on the CS surface.

In this study, ANPT showed a good inhibition performance for every experiment at a concentration of 200 ppm.

### 3.10 Synergistic Effect in Presence of Surfactant

In presence of suitable surfactants, the efficiency of organic inhibitors can be enhanced through a synergistic effect [29-30]. CTAB is a cationic surfactant and a quaternary ammonium salt. It contains a long hydrocarbon chain and is used as an inhibitor as well as biocides [29]. Furthermore, the large molecular weight and negative charge on bromide ions facilitate CTAB to adsorb on the CS surface through Van der Waal's force. The effect of the addition of CTAB with ANPT in 0.5 M HCl solution to inhibit CS corrosion in acid solution is measured by the following electrochemical tests:

#### 3.10.1 OCP Analysis

**Figure 3. 15** shows the OCP curves of the CS electrode in 0.5M HCl solution in the absence and presence of ANPT in combination with CTAB.

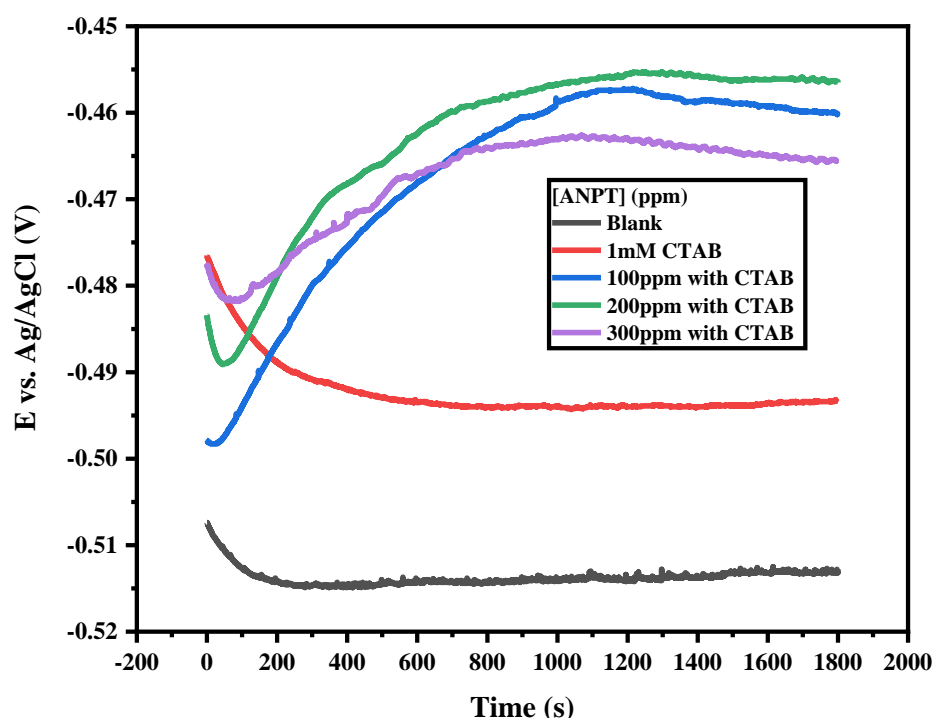


**Figure 3. 15** Time variation of the OCP for CS in 0.5 M HCl solution with different concentrations of ANPT in combination with 1 mM CTAB at room temperature

Initially, the OCP value of the CS electrode in inhibitor-free 0.5 M HCl solution seems to be negative shown in OCP graph signifying CS dissolution and with the addition of 1mM CTAB, the OCP value shifted toward positive value presented in **Figure 3. 15**. This indicates the decrease in the deposition of corrosion products on the CS surface in presence of CTAB. Moreover, the electrode's potential shifts toward higher negative values than the initial potential indicating the dissolution of the CS electrode in both 0.5 M HCl solution and 1 mM CTAB solution [24-25]. After 300 seconds the change in potential is observed almost steady.

The curves for 100 ppm, 200 ppm and 300 ppm in the figure represents the variation in OCP of CS in 0.5 M HCl with time after the addition of ANPT in presence of 1 mM CTAB at room temperature, respectively. All these curves show a more positive value of OCP than curves of blank solution and 1 mM CTAB . Initially, all the curves moved toward a negative value indicating CS dissolution, after around 150 seconds an upper trend is observed indicating a decrease in metal dissolution [25]. Almost after 1100 seconds a steady change is observed in all the curves. So, these results attributed that the ANPT mixed with 1Mm CTAB formed a protective film on the CS surface immersed in 0.5 M HCl solution. Moreover, at a concentration of 200 ppm of ANPT in 0.5 M HCl with 1 Mm CTAB solution the most positive OCP value of CS is found indicating a better *IE* than the other concentrations.

### 3.10.2 PDP Analysis

**Figure 3. 16** shows the cathodic and anodic polarization curve of CS in 0.5 M HCl in the absence and presence of various concentrations of ANPT mixed with 1mM CTAB at room temperature. The scan rate was  $0.5 \text{ mVs}^{-1}$ .

The values of corrosion potential ( $E_{\text{corr}}$ ), cathodic and anodic Tafel slope ( $\beta_c$  and  $\beta_a$ ) and corrosion current density ( $i_{\text{corr}}$ ), obtained by extrapolation of the Tafel lines, are presented in **Table 3. 13**.

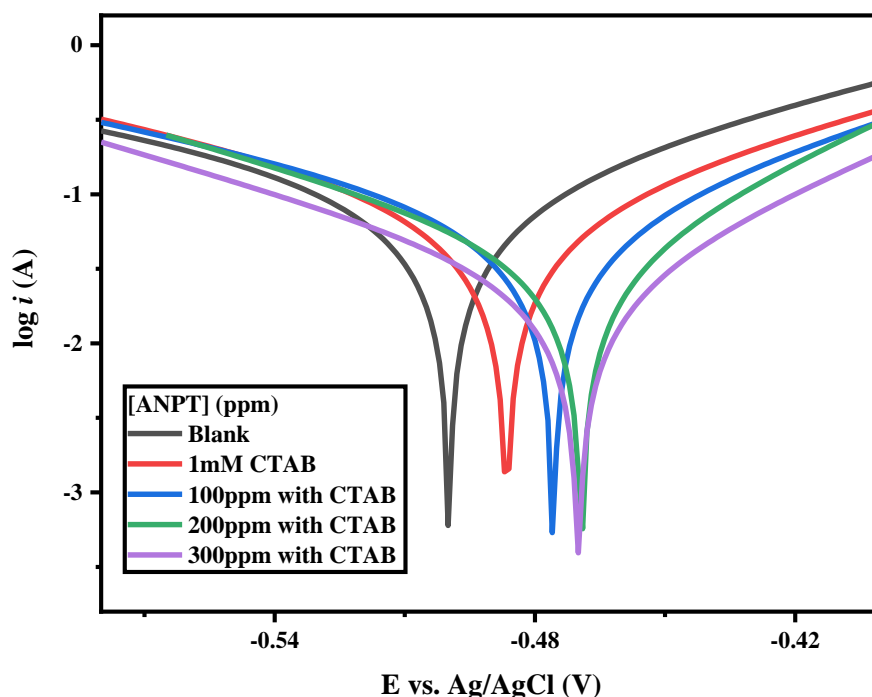


**Figure 3. 16** PDP plots for CS in 0.5 M HCl solution with different concentrations of ANPT in presence of 1 mM CTAB at room temperature

This figure illustrates how the concentration of thiadiazole derivatives affects the cathodic and anodic branches, respectively, and how this influence varies in presence of 1 mM CTAB. The  $IE_{PDP}$  of ANPT for CS against 0.5 M HCl by adding 1 mM CTAB at room temperature has been calculated by using equation (7) [6, 28].

**Table 3. 13** The PDP parameters for CS in 0.5M HCl solution with different concentrations of ANPT in presence of 1 mM CTAB at room temperature

$C_{inh}$ (ppm)	$E_{corr}$ (mV)	$i_{corr}$ ( $\text{mA cm}^{-1}$ )	$\beta_c$ ( $\text{mVdec}^{-1}$ )	$\beta_a$ ( $\text{mVdec}^{-1}$ )	$IE_{PDP}$ (%)
<b>Blank</b>	-499.80	1.3	209.6	130.6	0.00
<b>1 mM CTAB</b>	-486.51	0.89	162.9	133.8	31.53
<b>100 + 1 mM CTAB</b>	-475.78	0.74	166.9	115.7	43.07
<b>200 + 1 mM CTAB</b>	-469.29	0.38	117.9	75.6	70.76
<b>300 + 1 mM CTAB</b>	-470.00	0.26	117.7	80.3	80.00

This table shows the  $E_{corr}$  displacements in the presence and absence of ANPT with 1mM CTAB towards positive value. Furthermore, a more increased in  $IE$  % of ANPT



is observed with the addition of 1 mM CTAB. This indicates that the absorption of corrosion inhibitor molecules on the surface of the metal sample led to the formation of a layer of protection on the CS surface is influenced by CTAB [28, 30].

Additionally, the values of  $\beta_c$  &  $\beta_a$  in the presence of ANPT mixed with CTAB considerably alter with the inhibitor's concentration, suggesting that these substances have an impact on the kinetics of the anodic and cathodic processes [5]. As can be seen in **Table 3. 13**, the  $IE$  increased with the increase in the concentration of ANPT mixed with 1 mM CTAB in 0.5M HCl solution. The best  $IE$  is observed at a concentration of 300ppm ANPT with CTAB and the  $IE_{PDP}$  is 80 %. Moreover, an inhibitor may only be classified as anodic or cathodic if its  $E_{corr}$  displacement is higher than 85 mV [25]. In this table, the maximum  $E_{corr}$  displacement in presence of 200 ppm ANPT is 29 mV, indicating that the mixture of ANPT & CTAB is a mixed-type inhibitor.

Now it is clear from the above discussion of PDP measurement that the presence of surfactant, CTAB enhances the IE of ANPT and the mixture worked as a mixed-type corrosion inhibitor.

### 3.10.3 FE-SEM Analysis of CS Surfaces

FE-SEM was used to examine the CS surface morphology in the absence and presence of ANPT in 0.5 M HCl solution with 1 mM CTAB [10, 11]. **Figure 3. 17** shows the FE-SEM images at 10  $\mu\text{m}$  magnification of normal CS surface, corroded CS surface dipped in 0.5 M HCl solution, CS surface dipped in 0.5 M HCl solution in presence of 200 ppm ANPT and surface immersed in 0.5 M HCl solution with 1mM CTAB in presence of 200 ppm ANPT.

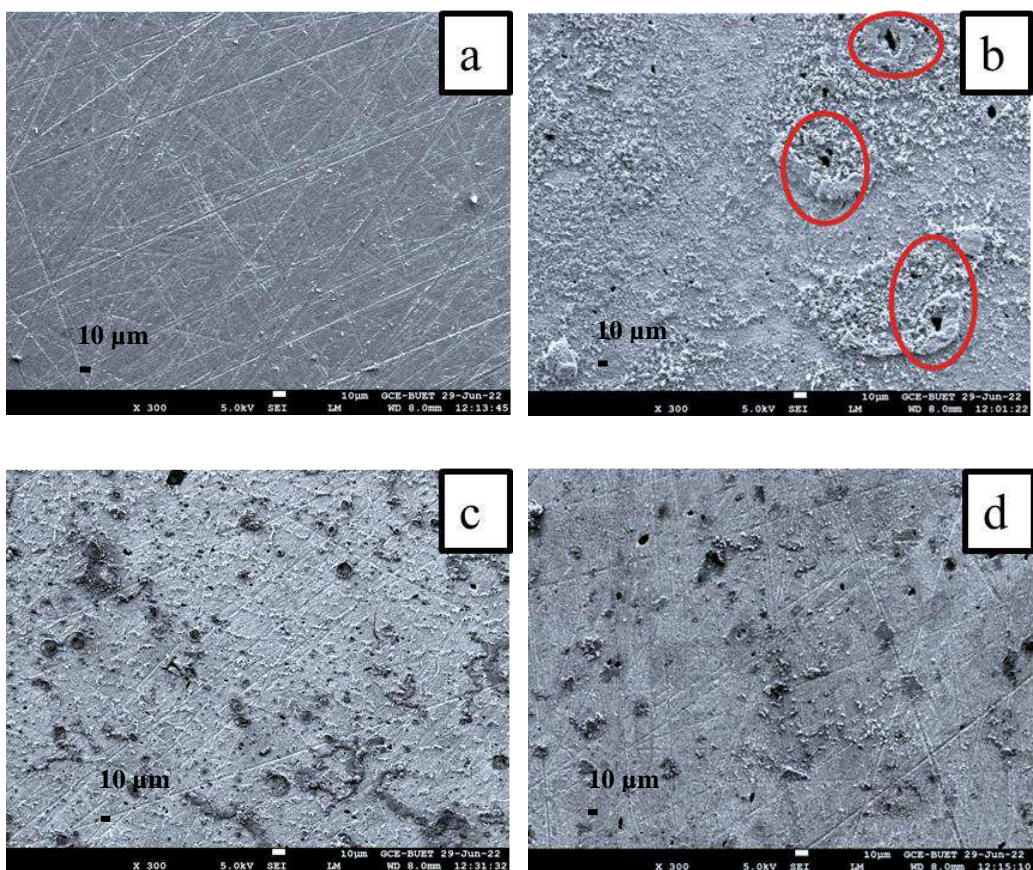


**Figure 3. 17** SEM of CS surface (a) before immersion (b) corroded surface after immersion 0.5 M HCl solution (c) in presence of 200 ppm ANPT (d) in presence of 200 ppm along with 1 mM CTAB

Here, image (a) presents a clean smoother surface, (b) shows a severely damaged surface with rust on it and a less damaged surface is observed in the image (c). In corporation with CTAB a more clearer surface is also found (d). These results demonstrated that inhibitors in presence of CTAB formed a surface-adsorbed layer that shields the CS from acid attack and inhibits the material's breakdown, thereby reducing corrosion. CTAB facilitates the ANPT molecule to adsorb on the CS surface more frequently resulting in enhanced *IE* of ANPT.

After performing all the tests a possible inhibition mechanism of ANPT in 0.5 M HCl in absence and presence of 1 mM CTAB for the CS surface has been preposed.

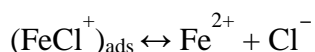
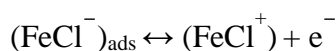
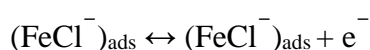
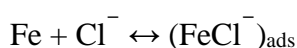
### 3.11 Proposed Corrosion Inhibition Mechanism

From the above discussion of the weight-loss test and electrochemical measurement, it's obvious that the inhibition mechanism of ANPT in 0.5 M HCl is followed by

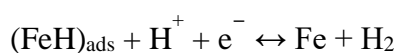
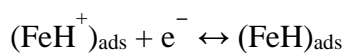
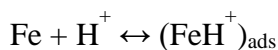
adsorption on CS surface. The initial stage in the mechanism of the inhibitor action is generally accepted to be the adsorption of organic inhibitors at the metal surface contact. Four different mechanisms exist for organic molecules to adsorb on metal surfaces,

- i. electrostatic interaction between the charged molecules and the charged metal
- ii. interaction of unshared electron pairs in the molecule with the metal
- iii. interaction of  $\pi$ -electrons with the metal and
- iv. a combination of types (i–iii) [17]

CS corrodes as a result of the Fe atoms breaking down into positive ions and electrons [29]. The simultaneous electrochemical processes of iron oxidation and hydrogen evolution occur on the anodic and cathodic sites of the steel surface in an acidic solution [32]. The anodic dissolution of iron follows the steps [33]:



The cathodic reaction is the conversion of  $\text{H}^+$  ions to molecular hydrogen during the corrosion of iron in a strong acid solution according to reaction mechanism given below [5]:



Thiadiazole derivative, ANPT contains polar group such as nitrogen and sulphur along with aromatic ring, amine group and nitro group having high electron density. This electron density is adsorbed on the CS surface through electrostatic force. Thus, through the electron density, ANPT acts as a protonated layer on the surface of CS and builds a

barrier between the CS surface and corrosive 0.5 M HCl acid media [29-33]. In **Figure 3. 18** the inhibition mechanism has been shown.

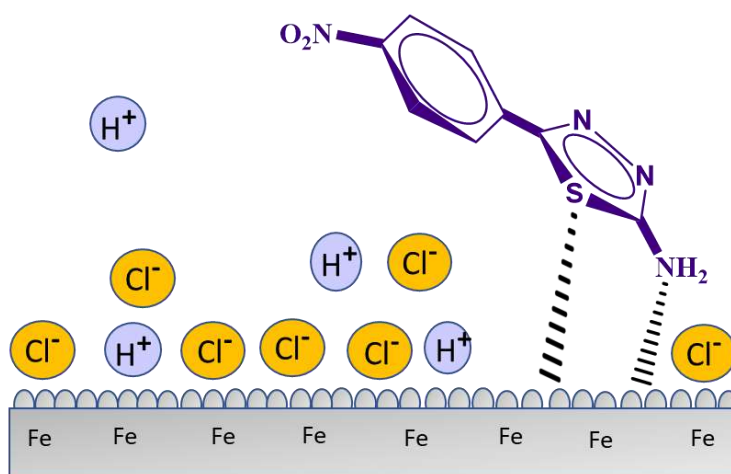


**Figure 3. 18** Inhibition mechanism of ANPT on the CS surface against HCl

The cationic surfactant, CTAB carries a positive charge and a negatively charged bromide ion in the acidic solution. This causes the adsorption of bromide ions onto the CS surface and the orientation of the dipoles of the surface compound with their negative ends towards the solution. As a result, the ionized CTAB easily reaches the CS surface preventing the direct acid solution attack [27] shown in **Figure 3. 19**. Moreover, the polar head acts as an adsorption mediator facilitating the adsorption of inhibitor, ANPT molecules [34].

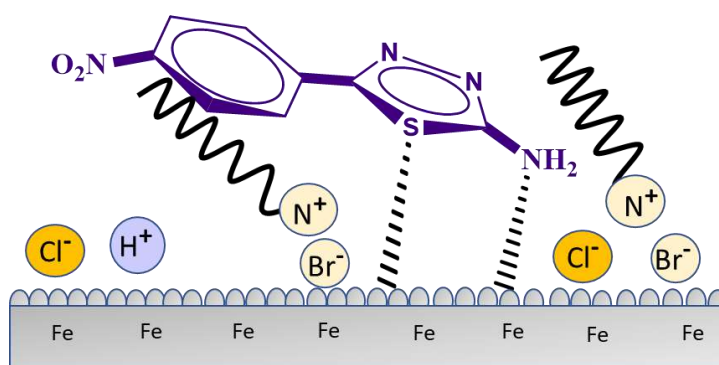


**Figure 3. 19** Inhibition mechanism of ANPT on the CS surface in presence of CTAB against HCl

## References

- [01] CT Keerthi Kumar, J. Keshavayya, T.N. Rajesh, S.K. Peethambar and A.R. Shoukat Ali, "Synthesis, characterization, and biological activity of 5-phenyl-1, 3, 4-thiadiazole-2-amine incorporated azo dye derivatives," *Org. Chem. Int.*, vol. 2013, pp. 1-7, 2013.
- [02] M. Amir, A. Kumar, I. Ali and S.A. Khan, "Synthesis of pharmaceutically important 1, 3, 4-thiadiazole and imidazolinone derivatives as antimicrobials," *Indian J. Chem.*, vol. 48B, pp. 1288-1293, 2009.
- [03] G. TrabANELLI, "1991 Whitney Award Lecture: Inhibitors-An Old Remedy for a New Challenge," *Corros.*, vol. 47, pp. 410-419, 1991.
- [04] H. Ouici, M. Tourabi, O. Benali, C. Selles, C.nJama, A. Zarrouk and F. Bentiss, "Adsorption and corrosion inhibition properties of 5-amino 1,3,4-thiadiazole-2-thiol on the mild steel in hydrochloric acid medium: Thermodynamic, surface and electrochemical studies," *J. Electroanal. Chem.*, vol. 803, pp. 125-134, 2017.
- [05] S. Varvara, L. M. Muresan, K. Rahmouni, and H. Takenouti, "Evaluation of some non-toxic thiadiazole derivatives as bronze corrosion inhibitors in aqueous solution," *Corros. Sci*, vol. 50, pp. 2596-2604, 2008.
- [06] I. A. Annon, A.S. Abbas, W.K. Al-Azzawi, M.M. Hanoon, A. Alamiery, W.N.R. Isahak and A.A.H. Kadhum, "Corrosion inhibition of mild steel in hydrochloric acid environment using thiadiazole derivative: Weight loss, thermodynamics, adsorption and computational investigations," *S. Afr. J. Chem. Eng.*, vol. 41, pp. 244-252, 2022.
- [07] F. Bentiss, M. Lebrini, and M. Lagrenée, "Thermodynamic characterization of metal dissolution and inhibitor adsorption processes in mild steel/2,5-bis(n-thienyl)-1,3,4-thiadiazoles/ hydrochloric acid system," *Corros. Sci*, vol. 47, pp. 2915-2931, 2005.
- [08] Y. Tang, F. Zhang, S. Hu, Z. Cao, Z. Wu, and W. Jing, "Novel benzimidazole derivatives as corrosion inhibitors of mild steel in the acidic media. Part I: Gravimetric, electrochemical, SEM and XPS studies," *Corros. Sci*, vol. 74, pp. 271-282, 2013.

- [09] M. Palomar-Pardavé, M. Romero-Romo, H. Herrera-Hernández, M.A. Abreu-Quijano, N.V. Likhanova, J. Uruchurtu, and J.M. Juárez-García, "Influence of the alkyl chain length of 2 amino 5 alkyl 1,3,4 thiadiazole compounds on the corrosion inhibition of steel immersed in sulfuric acid solutions," *Corros. Sci.*, vol. 54, pp. 231–243, 2012.
- [10] S. Martinez and I. Stern, "Thermodynamic characterization of metal dissolution and inhibitor adsorption processes in the low carbon steel/mimosa tannin/sulfuric acid system," *Appl. Surf. Sci.*, vol. 199, pp. 83-89, 2002.
- [11] F. Bentiss, M. Bouanis, B. Mernari, M. Traisnel, H. Vezin, and M. Lagrenée, "Understanding the adsorption of 4H-1,2,4-triazole derivatives on mild steel surface in molar hydrochloric acid," *Appl. Surf. Sci.*, vol. 253, pp. 3696–3704, 2007.
- [12] E. Ituen, O. Akaranta, and A. James, "Evaluation of Performance of Corrosion Inhibitors Using Adsorption Isotherm Models: An Overview," *Chem. Sci. Int. J.*, vol. 18, pp. 1–34, 2017.
- [13] Y. M. Tang, W. Z. Yang, X. S. Yin, Y. Liu, R. Wan, and J. T. Wang, "Phenyl-substituted amino thiadiazoles as corrosion inhibitors for copper in 0.5 M H<sub>2</sub>SO<sub>4</sub>," *Mater. Chem. Phys.*, vol. 116, pp. 479–483, 2009.
- [14] A. Kokalj, "Corrosion inhibitors: physisorbed or chemisorbed?," *Corros. Sci.*, vol. 196, pp. 109939, 2022.
- [15] Y. M. Abdulsahib, A.J.M. Eltmimi, S.A. Alhabeeb, M.M. Hanoon, A.A. Al-Amiery, T. Allami and A.A.H. Kadhum, "Experimental and theoretical investigations on the *IE* of n-(2,4-dihydroxytolueneylidene)-4-methylpyridin-2-amine for the corrosion of mild steel in hydrochloric acid," *Int. J. Corros. Scale Inhib.*, vol. 10, pp. 885–899, 2021.
- [16] N. O. Obi-Egbedi and I. B. Obot, "Adsorption behavior and corrosion inhibitive potential of xanthene on mild steel/sulphuric acid interface," *Arab. J. Chem.*, vol. 5, pp. 121–133, 2012.
- [17] F. S. de Souza and A. Spinelli, "Caffeic acid as a green corrosion inhibitor for mild steel," *Corros. Sci.*, vol. 51, pp. 642–649, 2009.
- [18] A. K. Singh and M. A. Quraishi, "The effect of some bis-thiadiazole derivatives on the corrosion of mild steel in hydrochloric acid," *Corros. Sci.*, vol. 52, pp. 1373–1385, 2010.

- [19] A.A. Fouda, K. Shalabi, A. S. Fouda, K. Shalabi, and R. Ezzat, "Evaluation of some thiadiazole derivatives as acid corrosion inhibitors for carbon steel in aqueous solutions," *J. Mater. Environ. Sci*, vol. 6, pp.1022-1039, 2015.
- [20] S. T. Keera and M. A. Deyab, "Effect of some organic surfactants on the electrochemical behaviour of carbon steel in formation water," *Colloids Surf. A: Physicochem. Eng. Asp.*, vol. 266, pp. 129–140, 2005.
- [21] A. K. Singh and M. A. Quraishi, "Effect of Cefazolin on the corrosion of mild steel in HCl solution," *Corros. Sci*, vol. 52, pp. 152–160, 2010.
- [22] G. M. Al-Senani, "Corrosion Inhibition of Carbon Steel in acidic chloride medium by Cucumis Sativus (cucumber) Peel Extract," *Int. J. Electrochem. Sci*, vol. 11, pp. 291-302, 2016.
- [23] W. S. Tait, "Electrochemical corrosion basics," in Handbook of Environmental Degradation Of Materials: Third Edition, *William Andrew Publishing*, pp. 97–115, 2018.
- [24] M. B. Radovanović, Ž. Z. Tasić, M. B. P. Mihajlović, A. T. Simonović, and M. M. Antonijević, "Electrochemical and DFT studies of brass corrosion inhibition in 3% NaCl in the presence of environmentally friendly compounds," *Sci. Rep.*, vol. 9, pp. 16081, 2019.
- [25] H. A. El-Dahan, T. Y. Soror, and R. M. El-Sherif, "Studies on the inhibition of aluminum dissolution by hexamine-halide blends Part I. Weight loss, open circuit potential and polarization measurements," *Mater. Chem. Phys.*, vol. 89, pp. 260–267, 2005.
- [26] H. J. Habeeb, H. M. Luaibi, R. M. Dakhil, A. A. H. Kadhum, A. A. Al-Amiery, and T. S. Gaaz, "Development of new corrosion inhibitor tested on mild steel supported by electrochemical study," *Results Phys.*, vol. 8, pp. 1260–1267, 2018.
- [27] A. Singh, E. E. Ebenso, and M. A. Quraishi, "Theoretical and Electrochemical Studies of Metformin as Corrosion Inhibitor for Mild Steel in Hydrochloric Acid Solution," *Int. J. Electrochem. Sci*, vol. 7, pp. 4766-4779, 2012.
- [28] D.V. Ribeiro and J.C.C. Abrantes, "Application of electrochemical impedance spectroscopy (EIS) to monitor the corrosion of reinforced concrete: A new approach," *Constr Build Mater.*, vol. 111, pp. 98-104, 2016.

- [29] A. Zarrouk, "Moroccan Journal of Chemistry Synergistic effect of halides and surfactants on the corrosion inhibition of thiazolo thiadiazole derivative for mild steel in acid medium," *Mor. J. Chem.*, vol. 5, pp. 164–176, 2017.
- [30] M. Mobin, M. Parveen, and M. Z. A. Rafiquee, "Synergistic effect of sodium dodecyl sulfate and cetyltrimethyl ammonium bromide on the corrosion inhibition behavior of L-methionine on mild steel in acidic medium," *Arab. J. Chem.*, vol. 10, pp. S1364–S1372, 2017.
- [31] Ulick R. Evans and C. V. King, "The Corrosion and Oxidation of Metals," *J. Electrochem. Soc.*, vol. 108, pp. 94C, 1961.
- [32] O. Olivares-Xometl, N.V. Likhanova, N. Nava, A.C. Prieto, I.V. Lijanova, A. Escobedo-Morales and C. López-Aguilar, "Thiadiazoles as corrosion inhibitors for carbon steel in H<sub>2</sub>SO<sub>4</sub> solutions." *Int. J. of Electrochem. Sci.*, vol. 8, pp.735-752, 2013.
- [33] R. Solmaz, "Investigation of the inhibition effect of 5-((E)-4-phenylbuta-1,3-dienylideneamino)- 1,3,4-thiadiazole-2-thiol Schiff base on mild steel corrosion in hydrochloric acid," *Corros. Sci.*, vol. 52, pp. 3321–3330, 2010.
- [34] S. Rajendran, B.V. Apparao and N. Palaniswamy, "Synergistic and antagonistic effects existing among polyacrylamide, phenyl phosphonate and Zn<sup>2+</sup> on the inhibition of corrosion of mild steel in a neutral aqueous environment," *Electrochim. Acta*, vol. 44, pp. 533-537, 1998.



## **4. CHAPTER CONCLUSION**

#### 4.1 Conclusion:

The organic compound ANPT can be prepared through a facile one-pot synthesis route. It is a good CI for CS against dilute acidic media 0.5 M HCl. The *IE* increases with the increase in the concentration of ANPT in corrosive media. ANPT molecules cover the CS surface by physical adsorption process and inhibit the damage.

- ⇒ WL test showed that the *IE* was inhibitor concentration dependent and the highest *IE* (81 %) was at concentration 250 ppm with the minimum *CR*.
- ⇒ By thermodynamic test the values of activation energy  $E_a$ , enthalpy,  $\Delta H_{ads}^o$  and entropy,  $\Delta S_{ads}^o$  showed the adsorption of ANPT molecule on CS surface. In this test the maximum *IE* obtained at concentration 200 ppm.
- ⇒ The adsorption nature of the ANPT molecule on the CS surface in the dilute acidic solution obeys Langmuir's adsorption isotherm. The negative value of Gibb's free energy,  $\Delta G_{ads}^o$  signifies the spontaneous physisorption behavior of ANPT on the CS surface through electrostatic interaction.
- ⇒ The electrochemical tests ( OCP, PDP, EIS) showed that the ANPT molecule acted as a mixed-type inhibitor for CS surface in 0.5 M HCl with 56 % *IE*.
- ⇒ The addition of CTAB enhanced the *IE* of ANPT through the synergistic effect.
- ⇒ It has been observed that the corrosion *IE* of ANPT was improved to 70 % by adding a low concentration of CTAB.
- ⇒ FE-SEM result showed a less corroded surface of CS after adding 200 ppm ANPT in the corrosive media. Further addition of 1 mM CTAB with 200 ppm ANPT provided a more smooth surface in the acidic media.